Department of Pathology, Anatomy, and Cell Biology Faculty Papers

Department of Pathology, Anatomy, and Cell Biology

8-21-2020

# Dysregulation of RyR Calcium Channel Causes the Onset of Mitochondrial Retrograde Signaling

Anindya Roy Chowdhury
*University of Pennsylvania*

Satish Srinivasan
*University of Pennsylvania*

György Csordás
*Thomas Jefferson University*

György Hajnóczky
*Thomas Jefferson University*

Narayan G Avadhani
*University of Pennsylvania*

## Recommended Citation

**Article**

# Dysregulation of RyR Calcium Channel Causes the Onset of Mitochondrial Retrograde Signaling



Schematic Diagram: Calcium-Calcineurin mediated retrograde signaling involve in RYR channel activation
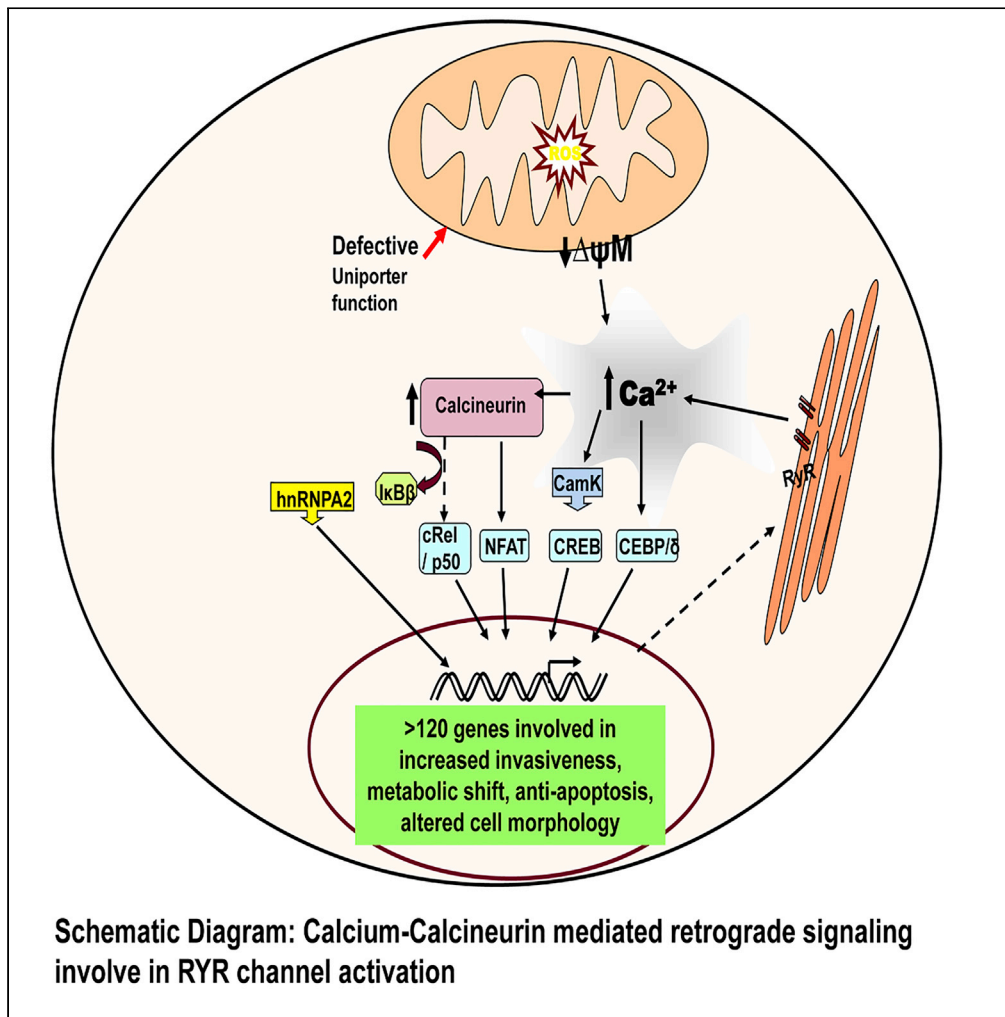
Anindya Roy
Chowdhury, Satish
Srinivasan, György
Csordás, György
Hajnóczky,
Narayan G.
Avadhani

narayan@vet.upenn.edu

**HIGHLIGHTS**

Multiple types of mitochondrial stress induce the expression of RyR channel genes

Stress-induced RyR channels are leaky, causing the release of $Ca^{2+}$ in the cytosol

Mitochondrial stress also impairs $Ca^{2+}$ uptake through mitochondrial uniporter

RyR antagonists blocked $Ca^{2+}$ leak, downstream signaling, and target gene expression

## Article

# Dysregulation of RyR Calcium Channel Causes the Onset of Mitochondrial Retrograde Signaling

Anindya Roy Chowdhury,[1,4] Satish Srinivasan,[1,3,4] György Csordás,[2] György Hajnóczky,[2] and Narayan G. Avadhani[1,5,*]

**SUMMARY**

**This study shows that multiple modes of mitochondrial stress generated by partial mtDNA depletion or cytochrome *c* oxidase disruption cause ryanodine receptor channel (RyR) dysregulation, which instigates the release of Ca$^{2+}$ in the cytoplasm of C2C12 myoblasts and HCT116 carcinoma cells. We also observed a reciprocal downregulation of IP3R channel activity and reduced mitochondrial uptake of Ca$^{2+}$. Ryanodine, an RyR antagonist, abrogated the mitochondrial stress-mediated increase in [Ca$^{2+}$]$_c$ and the entire downstream signaling cascades of mitochondrial retrograde signaling. Interestingly, ryanodine also inhibited mitochondrial stress-induced invasive behavior in mtDNA-depleted C2C12 cells and HCT116 carcinoma cells. In addition, co-immunoprecipitation shows reduced FKBP12 protein binding to RyR channel proteins, suggesting the altered function of the Ca$^{2+}$ channel. These results document how the endoplasmic reticulum-associated RyR channels, in combination with inhibition of the mitochondrial uniporter system, modulate cellular Ca$^{2+}$ homeostasis and signaling under mitochondrial stress conditions.**

## INTRODUCTION

Mitochondria (mt) are the powerhouse of cells as they produce most cellular ATP through respiration-linked oxidative phosphorylation. In addition to harnessing energy from food material, they participate in several essential cellular functions including the integration of metabolism; synthesis of intermediates for lipid, sterol, nucleotide, and amino acid synthesis; co-ordination of apoptotic signals; and production of signaling molecules such as reactive oxygen species (Friedman and Nunnari, 2014; Tait and Green, 2012). Another important function of mitochondria, in association with the endoplasmic reticulum (ER), is to modulate intracellular Ca$^{2+}$ homeostasis (Giorgi et al., 2009). The ER is the major reservoir of Ca$^{2+}$ in resting cells. Shuttling Ca$^{2+}$ from the ER to the mitochondria through the IP3 receptor calcium ion channel regulates ATP production to meet the cellular energy needs (Cardenas et al., 2010).

The mitochondrial function requires constant communication with the nucleus, which is achieved by tightly orchestrated signaling networks that control both the biogenesis and function of mitochondria (Guha and Avadhani, 2013; Yong and Tang, 2018). Mitochondrial biogenesis is maintained by anterograde signals from the nucleus to the mitochondria that control the import of proteins, mtDNA maintenance, and gene expression as demanded by the energy and growth requirements of the cell. Metabolic stress due to impaired mitochondrial respiration, partial or complete mtDNA depletion, disruption of cytochrome *c* oxidase (CcO) complex, suppression of mitochondrial transcription, and hypoxia can induce mitochondria-to-nucleus stress signaling pathway, called mitochondrial retrograde signaling (MtRS) (Butow and Avadhani, 2004; Guha and Avadhani, 2013). Recent research has focused on signaling initiated by mitochondria under stress to play a key role in cellular function and homeostasis (Yang and Kim, 2019). This could involve either physical or chemical stress, which ranges from acute to chronic. Mitochondrial stress signaling affecting nuclear gene expression brings about phenotypic changes in cell morphology, cell migration, and growth characteristics (Amuthan et al., 2001), which could make a change in stochastic cellular behaviors. Different MtRS signaling mechanisms have been reported in a variety of metazoan organisms and experimental contexts. The occurrence of MtRS has been reported in mtDNA mutations, deletions, recombinations, and mitochondrial unfolded protein response (mtUPR). The importance of MtRS has been implicated in multiple diseases including cancer progression, myopathies, neurodegeneration, and other disorders (Amuthan et al., 2001, 2002; Arnould et al., 2002; Desideri et al., 2015; Fang et al., 2010; He et al., 2010; Ishikawa et al., 2008).

[1]Department of Biomedical Sciences, School of Veterinary Medicine, University of Pennsylvania, Philadelphia, PA 19104, USA

[2]Mitocare Center, Department of Pathology, Anatomy and Cell Biology, Thomas Jefferson University, Philadelphia, PA 19107, USA

[3]Present address: Roche Molecular Systems, 1080, US-202, Branchburg, NJ 08876, USA

[4]These authors contributed equally

[5]Lead Contact

*Correspondence: narayan@vet.upenn.edu

https://doi.org/10.1016/j.isci.2020.101370

Intracellular $Ca^{2+}$ acts as a second messenger to regulate a wide range of cellular functions, including muscle contraction, neurotransmission, and regulation of transcription through activation of specific transcription factors (Clapham, 2007; Demaurex and Nunes, 2016). We and others have shown that increased $[Ca^{2+}]_c$ and activation of calcineurin (Cn) are integral components of the signaling cascade involved in MtRS (Biswas et al., 1999; Goffart and Wiesner, 2003). We also showed that partial mtDNA depletion, hypoxia, environmental toxins, and other factors that affect mitochondrial function and disrupt mitochondrial membrane potential ($\Delta\Psi_m$) initiate $Ca^{2+}$/Cn-dependent retrograde signaling (Srinivasan and Avadhani, 2007). One hallmark of this signaling is the elevation of $[Ca^{2+}]_c$, which is maintained by the ER and mitochondrial $Ca^{2+}$ stores (Rizzuto et al., 2012). Indeed, this intracellular organelle communication is functionally important for cellular metabolism and cell survival (Duchen, 1999; Franzini-Armstrong, 2007). Even though mitochondrial affinity for $Ca^{2+}$ is relatively low, they play a vital role in taking up $Ca^{2+}$ and releasing it back to the cytosol to regulate signaling (Giorgi et al., 2009; Rizzuto et al., 2012). Under conditions of impaired mitochondrial function and disruption of $\Delta\Psi m$, we showed increased steady-state $[Ca^{2+}]_c$ and activation of Cn, which in turn activates *NFAT*, *CREB*, *CEBPδ*, and a unique IkBβ-dependent nuclear factor-κB pathway (Biswas et al., 2005b). In addition, elevated $[Ca^{2+}]_c$ also activates many kinases such as PKC, CaMKIV (Arnould et al., 2002), JNK, and MAPK (Amuthan et al., 2002; Friis et al., 2014). Furthermore, the $Ca^{2+}$/Cn pathway activates heterogeneous nuclear ribonuclear protein *hnRNPA2*, which acts as a transcriptional co-activator for mitochondrial stress-induced transcription factors cRel:p50, *CREB*, *CEBPδ*, and *NFAT* (Guha et al., 2009). HnRNPA2 plays a critical role in the assembly or stability of enhanceosome complexes at promoter sequences leading to synergistic activation of >120 stress response genes (Biswas et al., 2005b; Guha and Avadhani, 2013) and telomere maintenance (Guha et al., 2018).

We have previously shown that partial depletion of mtDNA in C2C12 cells causes increased $[Ca^{2+}]_c$ and initiates MtRS (Biswas et al., 1999). However, the precise mechanism of altered $Ca^{2+}$ homeostasis in cells subjected to mitochondrial stress remains unresolved. In this study, we show that partial depletion of mtDNA or disruption of the CcO complex induces RyR1 and 3 $Ca^{2+}$ channel mRNA and protein expression. This is accompanied by a decrease in steady-state levels of FKBP12, a critical regulator of RyR $Ca^{2+}$ channel gating. Altered FKBP12-RyR binding is known to cause intracellular $Ca^{2+}$ leak, causing increased $[Ca^{2+}]_c$ and initiating MtRS (Dirksen and Avila, 2002; Marx et al., 2000). A steady transfer of $Ca^{2+}$ from the ER to mitochondria is vital for maintaining cellular bioenergetics (Green and Wang, 2010). We present evidence that mitochondrial dysfunction impairs $Ca^{2+}$ uniporter function and uptake of $Ca^{2+}$, leading to increased $Ca^{2+}$ pool in the cytosol. Furthermore, short hairpin RNA (shRNA)-mediated knockdown (KD) of *RyR1* mRNAs in cells with dysfunctional mitochondria reversed Cn activity and abrogated the signaling-associated transcription factor activation and gene expression, suggesting that overexpression of RyR $Ca^{2+}$ channel is a critical factor in the induction and maintenance of MtRS. This study provides a unified mechanism of altered $Ca^{2+}$ homeostasis in cells subjected to two different types of mitochondrial dysfunctional stress: mtDNA depletion and CcO4KD.

## RESULTS

### A Distinctive Agonist-Induced $Ca^{2+}$ Release Pattern in Cells with Dysfunctional Mitochondria

Previously, we showed that activation of Cn is an early step of MtRS in partial mtDNA-depleted C2C12 skeletal myoblasts and A549 lung carcinoma cells (Amuthan et al., 2001; Biswas et al., 1999). In the present study, we determined the role of mitochondrial dysfunction-induced changes in $Ca^{2+}$ homeostasis by using *CcO* subunit *IVi1*-silenced (CcO4KD) C2C12 cells and mtDNA depletion in HCT116 and C2C12 cells. The mtDNA contents of both C2C12 cells and HCT116 cells were reported before and also presented in Figures S1A and S1B. Figure S1 shows that 2′,3′-Dideoxycytidine (ddC; Millipore Sigma, D5782) or ethidium bromide treatment caused about 70%–80% reduction in mtDNA content in HCT116 and C2C12 cells by about 5–10 growth cycles. All primer information is provided in Table S1. The CcO4KD cells show reduced CcO activity, a marked metabolic shift toward glycolysis, and morphological changes similar to the mtDNA-depleted myoblasts described before (Srinivasan et al., 2016).

Acetylcholine is an agonist for IP3 receptor-induced $Ca^{2+}$ release, whereas caffeine sensitizes the RyR channel opening to induce $Ca^{2+}$ release (Pessah et al., 1987). These two agonists were used to trace the Ip3R- and RyR-mediated $Ca^{2+}$ release in live-cell imaging. Finally, an irreversible ER $Ca^{2+}$-ATPase inhibitor thapsigargin was used for the depletion of the ER $Ca^{2+}$ store. Intracellular free $Ca^{2+}$ concentration ($[Ca^{2+}]_i$) and $Ca^{2+}$ release properties were monitored and recorded using the fluorescent dye Fura-2-AM in individual cells. Acetylcholine (10 μM), caffeine (5 mM), and thapsigargin (2 μM) were added sequentially to control
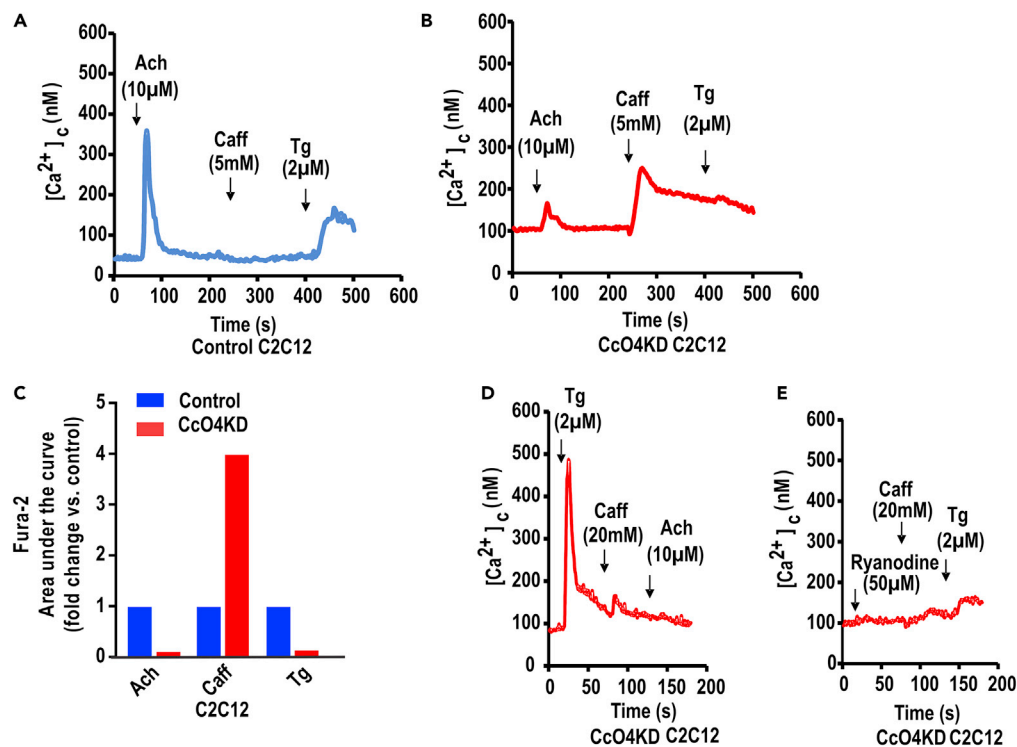
**Figure 1. CcO Disruption in C2C12 Cells Alters RyR and IP3R Agonist-Induced Ca$^{2+}$ Release**

(A–E) $[Ca^{2+}]_c$ measurements were carried out with control and CcO4KD cells as described in the Transparent Methods. Traces show the average response of three identical runs (average ≤ 30 cells/run) to different agonists in all cell lines. Recorded data were further analyzed by SpectralyzerLSMDeluxe version 2009092525 software to subtract the background fluorescence before calculating the $F_{380/340}$ ratio and finally represented as nanomolars. (A) Ca$^{2+}$ release in control cells. (B, D, and E) Ca$^{2+}$ release for CcO4KD cells. (C) The area under the curve of increases in $[Ca^{2+}]_c$ release in response to different agonists and inhibitors. The values (µM Ca$^{2+}$) are mean of tracings with >90 cells presented in (B, D, and E). Caff, caffeine; Ach, acetylcholine; Tg, thapsigargin.

and CcO4KD C2C12 cells as shown in Figures 1A and 1B (mean values of 30 cells in triplicate for each group). Control C2C12 cells showed a robust response to acetylcholine with a higher peak at 360 ± 25 nM ($[Ca^{2+}]_c$) (mean of 3 replicates and 30 cells per replicate, $p < 0.05$), compared with CcO4KD cells, which gave a peak at 166 ± 10 nM ($[Ca^{2+}]_c$). However, caffeine-stimulated sarcoplasmic reticulum (SR)-Ca$^{2+}$ release was detected only in CcO4KD cells where the ($[Ca^{2+}]_c$) was raised up to 249 nM ± 14 ($p < 0.001$) (Figures 1A and 1B). Figure 1C represents the area under the curve quantifications of Ca$^{2+}$ response with the aforementioned agonists in control and CcO4KD C2C12 cells (Figures 1A and 1B). The acetylcholine-mediated ($[Ca^{2+}]_c$) rise and ensuing recovery were faster in control cells compared with CcO4KD cells (Figure S2A). The response to caffeine was maximal with 5 mM as 20 mM caffeine (Figure S2B) did not induce a significantly higher $[Ca^{2+}]_c$ rise (Figure 1B).

ATP, another IP3-mobilizing agonist, duplicated the Ca$^{2+}$ mobilization pattern observed for acetylcholine in both CcO4KD and control cells (Figures S2C and S2D). The addition of caffeine after ATP (0.1 mM) induced similar $[Ca^{2+}]_c$ patterns to that for caffeine after acetylcholine. The role of the ryanodine receptor in caffeine-mediated calcium release was confirmed in experiments showing that ryanodine (50 µM), an antagonist of RyR channels, caused a decrease in the caffeine-mediated Ca$^{2+}$ release (Figure 1E). Similarly, depletion of the ER store by pretreatment with thapsigargin essentially eliminated the caffeine-mediated Ca$^{2+}$ release (Figure 1D). These results show that disruption of the CcO complex alters ER Ca$^{2+}$ release by downregulating the IP3R-dependent mechanism and upregulating the RyR-mediated pathway.

To test the similarity in response to multiple forms of mitochondrial stress, we also tested the agonist-induced Ca$^{2+}$ release in control and mtDNA-depleted colon carcinoma HCT116 cells. Figures 2A and 2B show that the peak area of ATP-induced Ca$^{2+}$ release is smaller in mtDNA-depleted cells compared
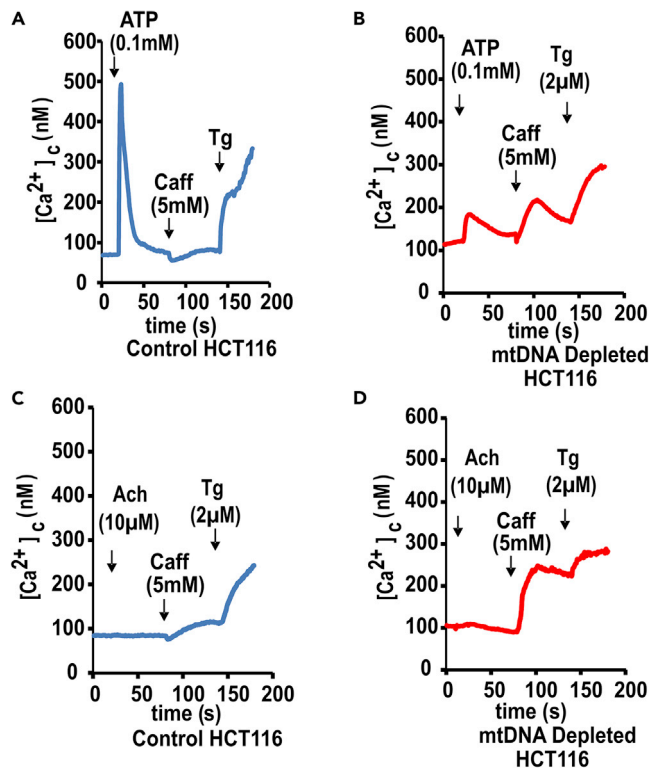
**Figure 2. Ca²⁺ Release in Response to RyR Channel and IP3R Channel Agonists in Partial mtDNA-Depleted HCT116 Cells**

(A–D) $[Ca^{2+}]_c$ measurements were carried out with control and mtDNA-depleted HCT116 cells as in Figure 1. Traces show the average response of three different runs (average ≤ 30 cells/run) following the addition of different agonists in all cell lines. Recorded data were further analyzed by SpectralyzerLSMDeluxe version 2009092525 software to subtract the background fluorescence before calculating the $F_{380/340}$ ratio and finally represented as nanomolars. (A and C) $Ca^{2+}$ release in control HCT116 cells in response to different agonists as indicated in figures. (B and D) $Ca^{2+}$ release in response to different agonists in mtDNA-depleted HCT116 cells. Caff, caffeine; Ach, acetylcholine; Tg, thapsigargin.

with control cells. However, treatment with caffeine following ATP stimulation evoked a $[Ca^{2+}]_c$ response only in mtDNA-depleted HCT116 cells but not in the control cells. Pretreatment with ryanodine completely abrogated caffeine response in mtDNA-depleted cells (not shown), suggesting the role of RyR channels in the altered pattern of $Ca^{2+}$ release. The addition of acetylcholine (10 μM) did not show $Ca^{2+}$ release in either control or mtDNA-depleted cells, suggesting the lack of muscarinic receptors. After treatment with acetylcholine, caffeine (5 mM) induced a markedly larger $Ca^{2+}$ release in mtDNA-depleted cells than in control cells (Figures 2C and 2D). Furthermore, the addition of thapsigargin (2 μM) caused activation of store-operated $[Ca^{2+}]_c$ rises in control and mtDNA-depleted cells (Figures 2A–2D). These results confirm that mitochondrial stress initiated by both mtDNA depletion and disruption of CcO complex sensitizes cells to RyR agonist-induced $Ca^{2+}$ release.

## Impaired Calcium Clearance by Dysfunctional Mitochondria

To test more directly the mechanism of the mitochondrial dysfunction-induced increase in the cytoplasmic $[Ca^{2+}]$, we measured the rate of mitochondrial $Ca^{2+}$ uptake in suspensions of saponin-permeabilized cells with Fura2-FF/FA dye. The influence of ER on $Ca^{2+}$ clearance was negated by pretreatment with thapsigargin. Dissipation of the $[Ca^{2+}]_c$ rise caused by a $Ca^{2+}$ bolus corroborates the $_{mt}Ca^{2+}$ uptake. Figures 3A and 3C show the time course of a 30 μM $CaCl_2$ pulse-induced mitochondrial $Ca^{2+}$ uptake and subsequent FCCP (carbonyl cyanide 4-trifluoromethoxy phenylhydrazone) addition, which fully releases the stored mitochondrial $Ca^{2+}$. The initial rate of $Ca^{2+}$ clearance following the addition of $CaCl_2$ in C2C12 and HCT116 cells is presented in Figures 3E and 3F. The $[Ca^{2+}]_c$ rise was cleared faster in control cells than in cells with dysfunctional mitochondria (Figures 3A, 3C, 3E, and 3F). Control C2C12 cell mitochondria removed $Ca^{2+}$ at 0.125 nM/s, whereas the clearance was nearly 30% slower in CcO4KD cells (Figure 3E). A similar decrease
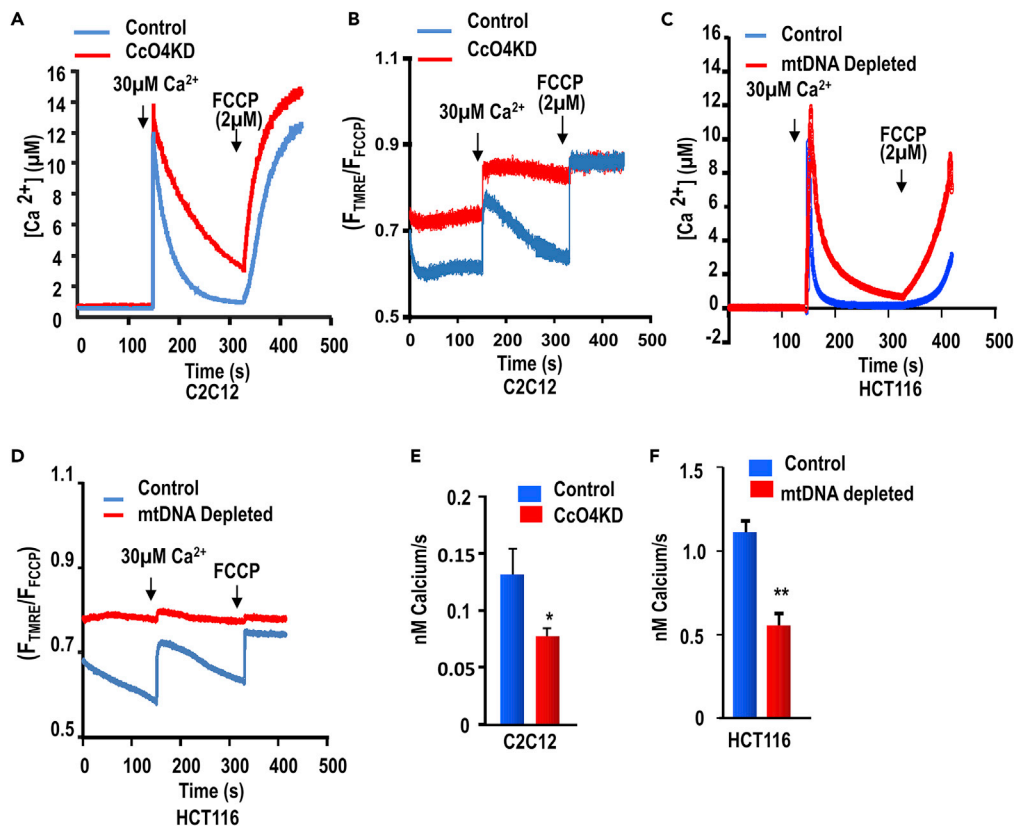
**Figure 3. Impaired Mitochondrial Ca²⁺ Clearance in CcO4KD and mtDNA-Depleted Cells**

Representative scans of $[Ca^{2+}]_c$ clearance by saponin-permeabilized cells following a 30 μM $CaCl_2$ spike in the presence of thapsigargin (2 μM). Recorded data were analyzed in PTI Felix and Felix GX software.

(A) $Ca^{2+}$ clearance in control and CcO4KD C2C12 cells.

(B) Tetramethylrhodamine (TMRE) fluorescence in control and CcO4KD C2C12 cells.

(C) $Ca^{2+}$ clearance in control and mtDNA-depleted HCT116 cells.

(D) TMRE fluorescence in control and mtDNA-depleted HCT116 cells.

(E) Rates of $Ca^{2+}$ uptake in control and CcO4KD C2C12 cells.

(F) Rates of $Ca^{2+}$ uptake by control and mtDNA-depleted HCT116 cells. Significance was calculated by one-way ANOVA with Tukey's multiple-comparison test, and data are presented as a mitochondrial dysfunctional group versus control. In all experiments, error bars represent standard deviations (*$p < 0.05$, **$p \leq 0.01$). Caff, caffeine; Ach, acetylcholine; FCCP, carbonyl cyanide 4-trifluoromethoxy phenylhydrazone; Tg, thapsigargin.

in $Ca^{2+}$ clearance rate was also seen in HCT116 cells following mtDNA depletion (Figures 3C and 3F). The $\Delta\Psi_m$ in both CcO4KD cells and mtDNA-depleted HCT116 cells was significantly lower than in the respective control cells with normal mtDNA contents or intact CcO complex (Figures 3B and 3D). Previously, we reported respiratory complex defects and reduced $\Delta\Psi_m$ in both CcO4KD cells (Srinivasan et al., 2016) and mtDNA-depleted HCT116 cells (Chowdhury et al., 2017). The mitochondrial respiratory chain defects in mitochondrial-associated deceased patients show reduced $\Delta\Psi_m$ along with reduced ATP synthesis, which in turn causes altered $[Ca^{2+}]_{mt}$ uptake under physiological stimulations (Visch et al., 2006). In conjunction with previous findings (Chowdhury et al., 2017; Srinivasan et al., 2016; Visch et al., 2006), these results show that cells with mitochondrial dysfunction indeed have disrupted $\Delta\Psi_m$ and a lower rate of mitochondrial $Ca^{2+}$ uptake that may represent the immediate upstream event for MtRS.

## Activation of Cn in Response to Mitochondrial Dysfunction

In addition to altered agonist-induced $Ca^{2+}$ release by cells with dysfunctional mitochondria (Figure 1), both CcO4KD C2C12 cells and mtDNA-depleted HCT116 cells also showed elevated steady-state $[Ca^{2+}]_c$ (Figures 4A and 4C). It is seen that the basal $Ca^{2+}$ level in CcO4KD cells increased to about 80 nM as opposed to 60 nM in control C2C12 cells (Figure 4A). Similarly, the steady-state $Ca^{2+}$ level
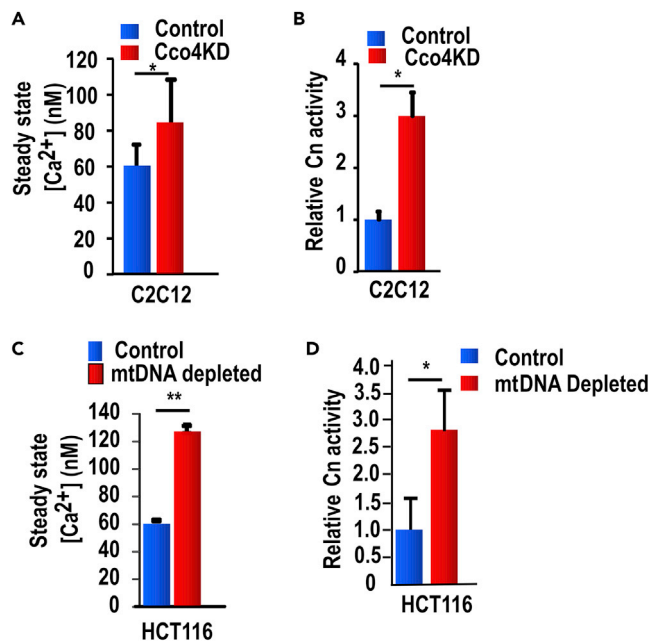
**Figure 4. Elevated Cytosolic Ca$^{2+}$ and Cn Activity in Response to Mitochondrial Dysfunction**

(A and B) (A) Basal [Ca$^{2+}$]$_c$ levels in control and CcO4KD C2C12 cells and (B) Cn activity in control and CcO4KD C2C12 cells.

(C and D) (C) Basal [Ca$^{2+}$]$_c$ levels in control and mtDNA-depleted HCT116 cells, and (D) Cn activity in control and mtDNA-depleted HCT116 cells. The bar diagrams represent the mean ± SEM from three independent experiments. Significance was calculated by one-way ANOVA with Tukey's multiple-comparison test, and data are presented as a mitochondrial dysfunctional group versus control. In all experiments error bars represent standard deviations (*$p < 0.05$, **$p \leq 0.01$).

increased in mtDNA-depleted HCT116 cells to about 130 nM from about 60 nM in control cells (Figure 4C). Consistent with the basal Ca$^{2+}$ increase, the Cn activity was increased nearly 3-fold in CcO4KD C2C12 cells and about 2.7-fold in mtDNA-depleted HCT116 cells (Figures 4B and 4D). This is consistent with our published reports (Srinivasan et al., 2016) that mRNA for the catalytic subunit of Cn (CnA) was increased by 2.5-fold in CcO4KD cells. These results show that in addition to altered agonist-induced Ca$^{2+}$ release, cells with dysfunctional mitochondria also show markedly increased Cn activity.

### Altered Ca$^{2+}$ Uniporter System Is Insufficient to Induce Retrograde Signaling

The mitochondrial uniporter complex (MCUC) is the major mitochondrial inner membrane system for the import of Ca$^{2+}$ from the cytoplasm (Baughman et al., 2011; Bick et al., 2012; Mammucari et al., 2017; Mishra et al., 2017). To understand the reason for inefficient Ca$^{2+}$ clearance associated with dysfunctional mitochondria in Figure 3, we assessed the levels of the three key components of the MCUC: MCU, MICU1, and EMRE (C22orf32). MCU is the main channel-forming protein for the transport of Ca$^{2+}$; EMRE is a mandatory scaffold that is required for MCU channel conductance, whereas MICU1 is a regulatory protein that mediates Ca$^{2+}$ gating (Kamer and Mootha, 2015) of MCU. As seen from Figures 5A and 5B, *MCU* mRNA levels were significantly reduced in mtDNA-depleted HCT116 cells, whereas there was no change in the *MICU1* mRNA level. Surprisingly, the *EMRE* mRNA level was increased in mtDNA-depleted cells (Figure 5C). A somewhat similar pattern of expression was seen in CcO4KD C2C12 myoblasts (Figure 5D), although the level of *MICU1* was also reduced significantly. Immunoblots in Figures 5E and 5F show that MCU protein level was decreased in mtDNA-depleted HCT116 cells, whereas the EMRE level was increased. The level of MICU1 was reduced marginally (Figure 5F). In CcO4KD C2C12 cells, both the MCU and MICU1 levels were significantly lower than in control cells in terms of both protein (Figure 5G) and mRNA levels (Figure 5D). However, as in HCT116 cells, the EMRE levels were higher than in control cells. These results suggest that altered uniporter abundance might contribute to the slower rate of Ca$^{2+}$ clearing. The levels of succinate dehydrogenase (SDHA) used as a mitochondrial loading control did not change significantly.
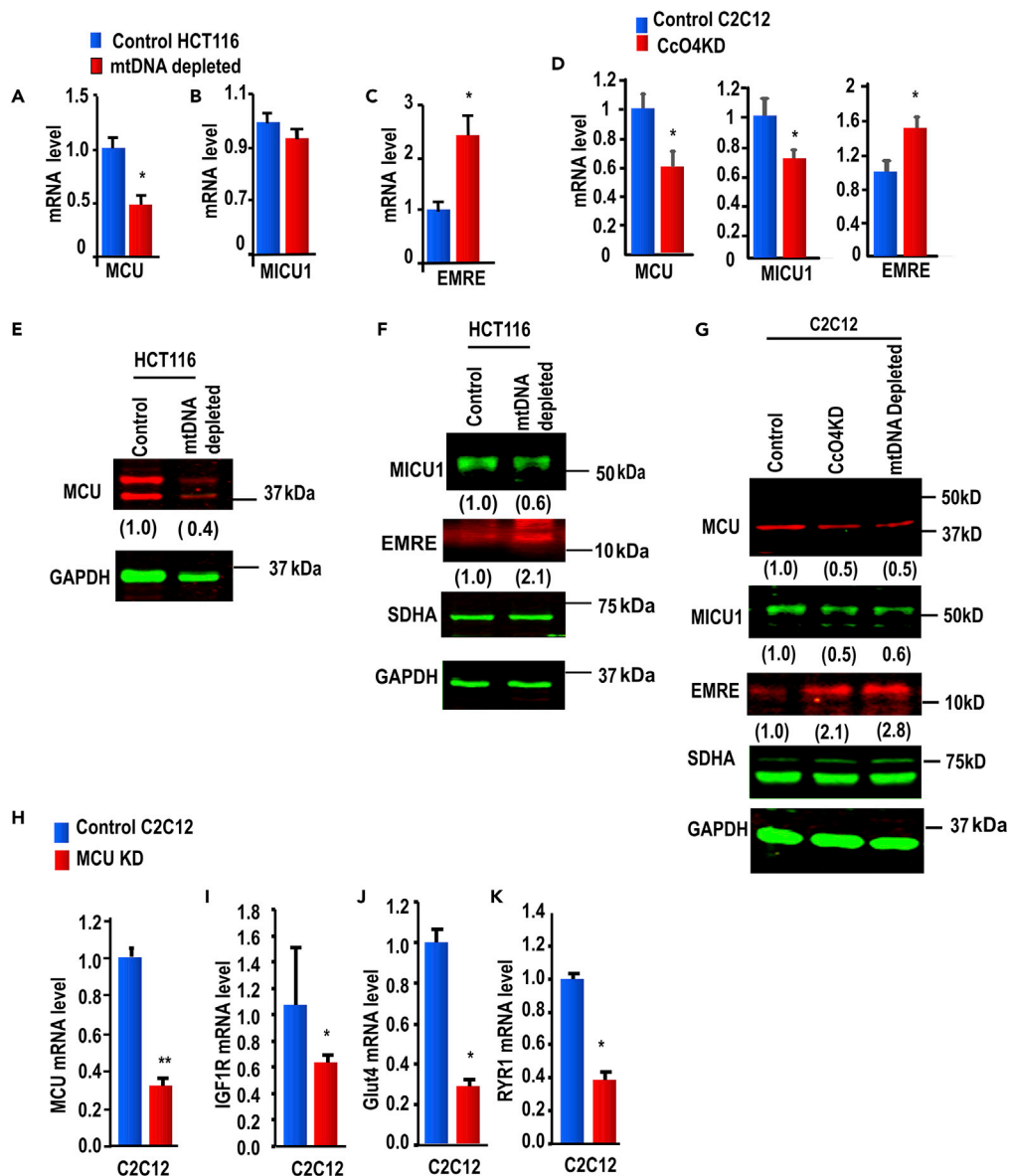
**Figure 5. Altered Mitochondrial Uniporter System in mtDNA-Depleted HCT116 Cells and CcO IVi1 KD C2C12 Cells**

(A–C) Levels of (A) *MCU*, (B) *MICU1*, and (C) *EMRE* mRNAs in control and mtDNA-depleted HCT116 cells.

(D) Quantitative mRNA analysis of *MCU, MICU1 and EMRE* in control and CcO4KD C2C12 cells.

(E and F) Immunoblot analysis of MCU, MICU1, and EMRE proteins from control and mtDNA-depleted HCT116. 30 μg proteins from whole-cell extracts were used in each case. Immunoblots were developed using respective primary (1:1,000 dilution) and 1:10,000 dilutions of secondary antibodies. The blots were imaged as described in the Transparent Methods. GAPDH was used as a loading control and SDHA as mitochondrial loading control.

(G) Relative protein levels of MCU, MICU1, and EMRE in control, CcO4KD, and mtDNA-depleted cells. GAPDH was used as a loading control and SDHA as mitochondrial loading control.

(H) Levels of MCU mRNA in control and stable MCU-specific shRNA-expressing (MCU-KD) cells.

(I, J, and K) The levels of (I) *IGF1R*, (J) *Glut4*, and (K) *RyR* (1,2, 3) mRNAs, respectively, in control and MCU-KD cells. Results represent the mean ± SEM from three separate experiments. Significance was calculated by one-way ANOVA with Tukey's multiple-comparison test, and data are presented as a mitochondrial dysfunctional group versus control. In all experiments error bars represent standard deviations (*p < 0.05, **p ≤ 0.01).
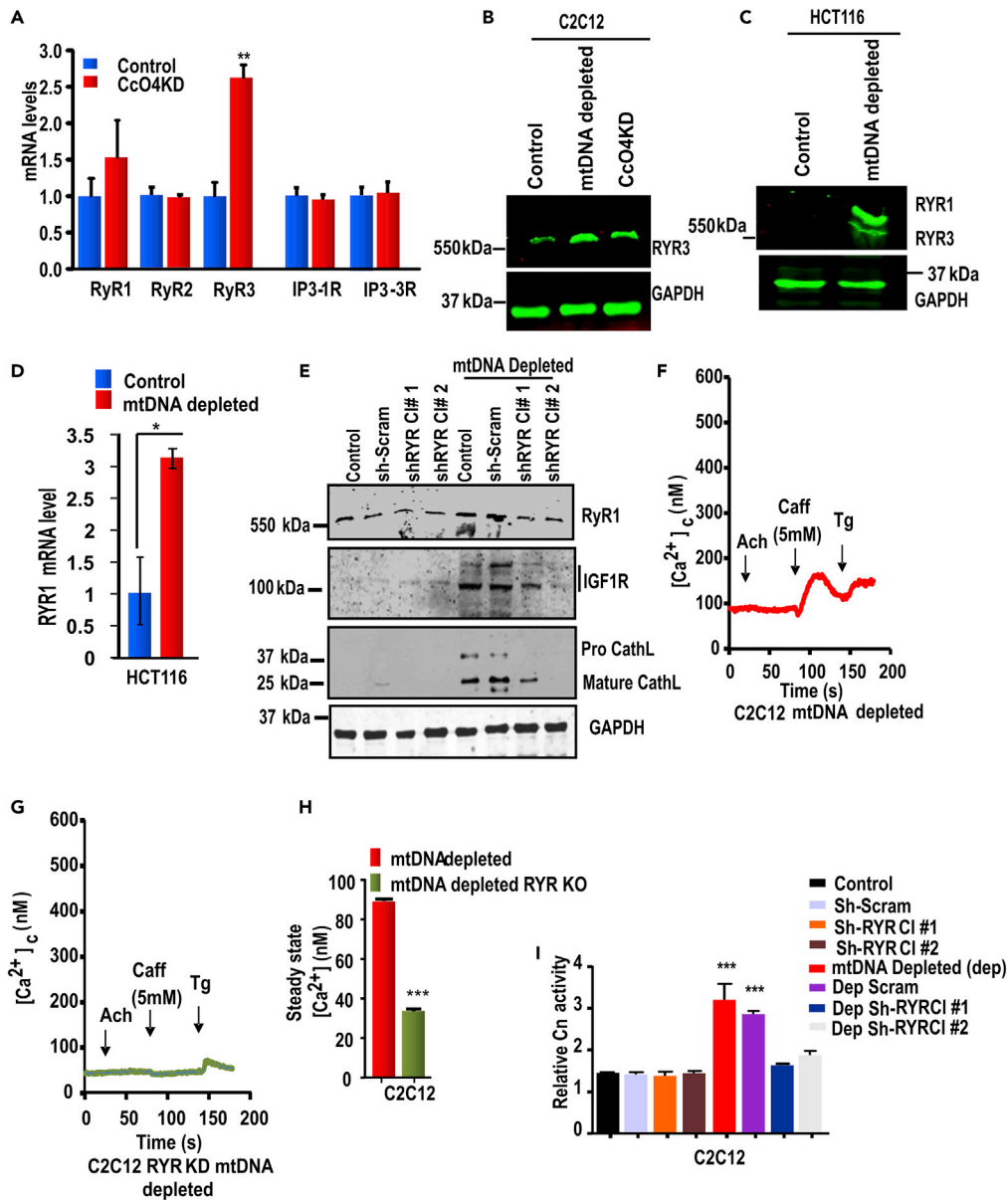
**Figure 6. Role of RyR Ca$^{2+}$ Channel Activation in Increased [Ca$^{2+}$]$_c$ in Response to Mitochondrial Stress**

(A) Real-Time PCR data on RyR and IP3R channel mRNA induction in CcO4KD C2C12 cells.

(B) Immunoblot data showing the induction of RyR protein level in control, mtDNA-depleted, and CcO4KD C2C12 cells. 50 μg protein was loaded in each lane, and GAPDH was used as the loading control.

(C) Immunoblot showing RyR1 and RyR3 induction in mtDNA-depleted HCT116 cells.

(D) The qPCR data showing induction of RyR mRNA in mtDNA-depleted HCT116 cells.

(E) Immunoblot analysis of proteins from control and mtDNA-depleted C2C12 cells expressing scrambled shRNA and two different RyR-specific shRNAs (named shRNA 1 or shRNA 2). Different molecular weight range areas of the same blot (~500 kDa, ~110 kDa, and about 40 kDa) were excised and probed with antibodies against RyR1, IGF1R, and cathepsin L proteins. GAPDH was used as a loading control.

(F and G) The agonist induced Ca$^{2+}$ release in (F) mtDNA-depleted and (G) mtDNA-depleted/RyR KD cells. Note that caffeine failed to induce Ca$^{2+}$ release in mtDNA-depleted/RyR KD cells. Traces show the average response of three identical runs (average ≤ 30 cells/run) following the addition of different agonists in each cell line. Recorded data were further analyzed by SpectralyzerLSMDeluxe version 2009092525 software to subtract the background fluorescence before calculate the F$_{380/340}$ ratio and finally represented as nM.

(H) The steady-state [Ca$^{2+}$]$_c$ levels in mtDNA-depleted and mtDNA-depleted/RyR KD cells. Caff, caffeine; Ach, acetylcholine; Tg, thapsigargin.

**Figure 6. Continued**

(I) Relative Cn activity in control, mtDNA-depleted C2C12 cells, and depleted cells expressing scrambled and specific shRNAs against all three RyR genes. Note that shRNA expression against RyR genes downregulated the activity. Mean ± SD was calculated from three independent experiments. Significance was calculated by one-way ANOVA with Tukey's multiple-comparison test, and data are presented as mitochondrial dysfunctional group versus control. In all experiments error bars represent standard deviations (*$p < 0.05$, **$p \leq 0.01$, ***$p \leq 0.001$).

To test if the reduced *MCU* mRNA played a direct role in inducing MtRs, we generated *MCU* KD cells by stably expressing shRNA for *MCU* mRNA in C2C12 cells (Figure 5H). We performed bioenergetic profile experiments with *MCU* KD and control cells to obtain respiratory parameters such as oxygen consumption rate (OCR), the percentage of oxygen consumption devoted to ATP production as well as the amount devoted to maintain the proton ($H^+$) leak (ECAR), and the maximal respiratory rate under conditions of un-coupled respiration. All the OCR and ECAR measurements were performed at 37°C under air and were re-corded simultaneously in an XF-24 analyzer platform. Figure S3A shows reduced basal as well as maximal respiration in MCU KD cells. Data were corrected by normalizing with total protein concentrations. We also calculated the ratio of ECAR/OCR as a measure of the relative magnitude of glycolysis versus oxidative phosphorylation. MCU KD cells showed elevated ECAR indicative of increased glycolysis and lactate pro-duction (Figure S3B). We tested transcriptional patterns of MtRS-specific marker genes such as insulin like growth factor 1 receptor (*IGF1R*), glucose transporter protein 4 (*Glut4*), and ryanodine receptor 1 (*RyR1*), which respond to mitochondrial respiratory stress signaling in different cells (Biswas et al., 1999, 2008b; Guha et al., 2007). Results in Figures 5H-5K show that all three markers of MtRS including mRNAs for *IGF1R*, *Glut4* and *RyR1* were downregulated in MCU KD cells. Thus, MCU mRNA KD and an associated reduction in $Ca^{2+}$ clearance alone are not sufficient to induce MtRS.

## The Role of RyR $Ca^{2+}$ Channels in Increased $[Ca^{2+}]_c$ and Activation of MtRS Marker Gene Expression

In compliance with increased caffeine-induced $Ca^{2+}$ release in cells with mitochondrial dysfunction in Fig-ures 1 and 2, *RyR3* mRNA and proteins were increased in CcO4KD C2C12 cells (Figures 6A and 6B) and both RyR1 and RyR3 proteins were induced in mtDNA-depleted HCT116 cells (Figures 6C and 6D). Notably, *IP3R* mRNA was not induced in CcO4KD cells. This is consistent with our previous report showing no increase in IP3R protein in mtDNA-depleted C2C12 cells (Biswas et al., 1999). As the RyR channels are known to be leaky (Dirksen and Avila, 2002; Marx et al., 2000), we reasoned that increased RyR expression may be the reason for increased cytosolic $Ca^{2+}$ levels. To test this possibility, we silenced all three *RyR* mRNAs using shRNA targeted to the common conserved region among all three genes. Figure 6E shows the levels of shRNA KD of *RyR* genes in control and mtDNA-depleted C2C12 cells. Immunoblots in Figure 6E show that the RyR protein levels were markedly lower in mtDNA-depleted cells stably transduced with shRNA expression vectors than in control cells and cells transduced with a scrambled shRNA expression vector (top panel). Levels of IGF1R (second panel from the top) and matured cathepsin L protein (second panel from the bottom) were also reduced in cells expressing *RyR* shRNA. Both these proteins are important markers of MtRS (Amuthan et al., 2001, 2002; Biswas et al., 1999; Guha et al., 2007). Control cells with normal mtDNA levels with or without expression of shRNA for *RyR* mRNAs do not express these genes (Figure 6E). These results confirm that increased *RyR* expression is essential for the initiation and/or propagation of MtRS.

To ascertain the role of RyR channel activity in the induced expression of MtRS target genes, we measured agonist-induced $Ca^{2+}$ release in RyR KD C2C12 cells. Figures 6F and 6G show the agonist-induced $Ca^{2+}$ release patterns in mtDNA-depleted (Figure 6F) and mtDNA-depleted/RyR KD (Figure 6G) C2C12 cells. RyR KD eliminated caffeine-mediated $Ca^{2+}$ release in mtDNA-depleted cells. Notably, the basal $[Ca^{2+}]_c$ level was reduced to ~38 nM in RyR KD cells from ~90 nM in mtDNA-depleted cells (Figure 6H). Consistent with the reduced $[Ca^{2+}]_c$, Cn activity was also reduced to control cell levels in mtDNA-depleted/RyR KD cells (Figure 6I). These results together show that induced activation of the RyR channel is a critical factor in the activation of Cn and downstream signaling cascade.

To further ascertain the role of induced or activated RyR $Ca^{2+}$ channel in inducing Cn activation and MtRS, which in turn induces cell proliferation and invasive behavior (Chowdhury et al., 2017; Srinivasan et al., 2016), we tested the effects of RyR channel KD in C2C12 cells in a scratch test (Figure S4) and the effects of RyR channel blocking with 50 μM ryanodine in C2C12 cells by Matrigel invasion (Figure 7A). Results show that KD of all three *RyR* mRNAs markedly reduced the migration of mtDNA-depleted
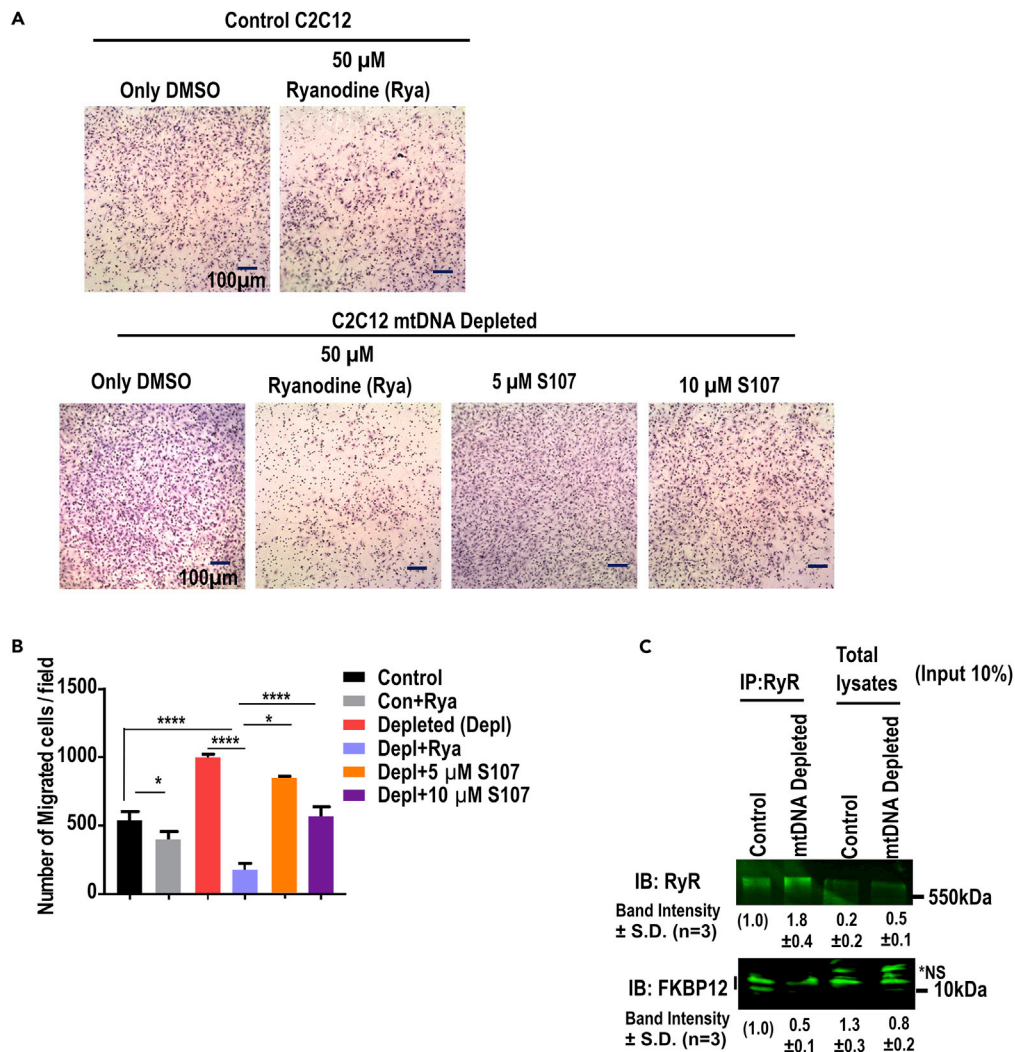
**Figure 7. Effects of RyR Channel Antagonists and Stabilizers on the Invasive Property of mtDNA-Depleted C2C12 Cells**

Ryanodine, an antagonist of RyR channels, and S107, an effective stabilizer of RyR1 and FKBP association, were used.

(A) Top panel: Matrigel invasion of control C2C12 cells treated with or without 50 μM ryanodine for 16 h before cells were loaded in the chamber. Lower panel: *In vitro* Matrigel invasion of mtDNA-depleted C2C12 cells treated with or without 50 μM ryanodine or different concentrations of RyR-FKBP stabilizer S107. Scale bars, 100 μM.

(B) Quantitation of invading cells from three separate experiments. The significance was calculated by one-way ANOVA with Tukey's multiple-comparison test, and data are presented as the treatment group versus no-treatment control. In all experiments error bars represent standard deviations ($*p < 0.05$, $****p \leq 0.001$).

(C) Immunoblot analysis (n = 3) of FKBP proteins coimmunoprecipitated with RyR from control and mtDNA-depleted C2C12 cells. The total lysate (Input) and immunoprecipitated proteins were probed with antibody to RyR and FKBP 12. IB, immunoblotting; IP, immunoprecipitation.

C2C12 cells in a scratch test (Figure S4). This assay revealed that the original scratch area was reduced by about 20% in control cells, whereas in mtDNA-depleted cells it was reduced by about 83% of the area in 24 h. There was no change in scrambled shRNA-expressing cells when compared with mtDNA-depleted cells, whereas *RyR* mRNA KD cells showed a remarkable recovery close to the control cell level (Figures S4A and S4B). Similarly, mtDNA-depleted C2C12 cells showed nearly 2-fold higher Matrigel invasion, which was effectively reduced by treatment with 50 μM ryanodine, an RyR antagonist that showed a marked reduction in Matrigel invasion as shown in Figures 7A and 7B. We also used different concentrations of (5 and 10 μM) cell-permeable derivative of S107, which marginally reduced the invasion of cells through Matrigel. S107 is known to block the leaky intracellular calcium release by stabilizing FKBP12 and

RyR associations. This treatment (Figure 7A, last two panels) significantly reduced the number of invasive cells compared with the mtDNA-depleted C2C12 cells. We further assessed the levels of FKBP12 association with RyR proteins by immunoprecipitation (Figure 7C). We found a marked increase in RyR protein in the immunoprecipitate and a considerably lower level of FKBP12 protein compared with that found in control cells. It has been reported that 1:1 stoichiometry of RyR and FKBP protein subunit, i.e., 4:4 is necessary for efficient regulation of tetrameric RyR channels (Brillantes et al., 1994; Meissner, 2010). In light of this, our results confirm that stress-induced RyR channels are leaky and responsible for increased $[Ca^{2+}]_c$, which is a critical factor in MtRS.

## DISCUSSION

Multiple mechanisms of mitochondria to nucleus cross talk have been described to explain changes in nuclear gene expression in response to mitochondrial genetic or metabolic defects (Butow and Avadhani, 2004; Yang and Kim, 2019). These include $Ca^{2+}$/Cn activation, mitochondrial unfolded protein response, mitochondrial reactive oxygen species-induced HIF1$\alpha$ or MAP kinase activation, and activation of micro-RNA (Butow and Avadhani, 2004; Carden et al., 2017; Guha and Avadhani, 2013). In previous studies, we showed that partial mtDNA depletion by chemical treatment of ethidium bromide or ddC caused a steady and sustained increase in the cytoplasmic $Ca^{2+}$, which in turn caused activation of protein phosphatase, Cn (Amuthan et al., 2001; Biswas et al., 1999, 2005b). In some cells, Cn activation occurred at the transcription level by inducing the expression of $Cn\ A\alpha$ mRNA, whereas in other cells, the activation was mostly post-translational through $Ca^{2+}$/calmodulin binding without a significant increase in transcription (Klee et al., 1979). This signaling cascade induced the expression of >120 nuclear genes involved in an array of cellular processes including plasma membrane receptors, cell cycle regulators, cytoskeletal proteins, and proteins associated with mitochondrial oxidative metabolism (Biswas et al., 2005b). We also showed that in immortalized cells, MtRS induced changes in cell morphology and invasive behavior, typical of tumor cells (Biswas et al., 2005a; Srinivasan et al., 2016). In this study, we elucidated the mechanism of altered $Ca^{2+}$ homeostasis in cells subjected to mitochondrial stress using partial mtDNA depletion and also $CcO$ subunit $IVi1$ mRNA silencing (CcO4KD) as stress inducers in two different cell lines. Our results show that a combination of altered uniporter function and markedly increased RyR $Ca^{2+}$ channel activity in response to mitochondrial stress together contribute to increased cytoplasmic $Ca^{2+}$ levels.

Mitochondria play a critical role in the regulation of cellular $Ca^{2+}$ homeostasis, mainly by acting as an important storage compartment (Bagur and Hajnoczky, 2017). The MCUC has been shown to be the main system for the transport of $Ca^{2+}$ released from IP3 and other channels in response to agonist-induced activation (Taylor and Tovey, 2010). We examined the MCUC components, and MCU was consistently downregulated in both cell types in response to mitochondrial stress. This is consistent with impaired $Ca^{2+}$ clearance by mitochondria from stressed cells. However, KD of $MCU$ alone did not induce MtRS markers, suggesting the need for other factors in inducing MtRS.

In extension of our previous observations in mtDNA-depleted C2C12 cells and A549 lung carcinoma cells (Amuthan et al., 2001; Biswas et al., 1999), we observed marked variations in the activity of RyR channels versus IP3R channels in cells with dysfunctional mitochondria. In control cells, there were high levels of $Ca^{2+}$ release in response to IP3 channel agonist acetylcholine, but no detectable $Ca^{2+}$ release in response to RyR channel agonist caffeine. In CcO4KD cells and mtDNA-depleted HCT116 cells, there was a marked reduction in acetylcholine-invoked $Ca^{2+}$ release, whereas caffeine invoked a 5- to 10-fold higher $Ca^{2+}$ release, suggesting a dramatic change in the inducibility or activity of these two channels. The overall $Ca^{2+}$ pool that is released from the ER in the control and CcO4KD cells appears to be similar as seen from the total $Ca^{2+}$ release invoked by ATP. Although the precise reason for this change in response to mitochondrial dysfunction remains unclear, it is most likely related to changes in the regulation of channels and also in the steady-state protein levels. We observed a large increase in RyR channel protein level and a corresponding increase in mRNA levels in response to the mitochondrial membrane or DNA damage. Similar patterns of $RyR$ mRNA and protein increase, as well as a large increase in caffeine-evoked $Ca^{2+}$ release, are observed in response to mitochondrial respiratory and metabolic inhibitors, including FCCP, antimycin A, oligomycin, and hypoxia (Biswas et al., 1999, 2008a; Srinivasan and Avadhani, 2007). Our results show that increased expression and altered activation of RyR $Ca^{2+}$ channels is a hallmark of mitochondrial dysfunction. Notably, IP3R-evoked $Ca^{2+}$ release is markedly reduced in cells with mitochondrial stress.

The three isoforms of RyR receptor $Ca^{2+}$ channels RyR1, RyR2, and RyR3 show nearly 70% homology in terms of amino acid sequences and are expressed in a cell- and tissue-specific manner. In C2C12 myocytes mostly RyR1 and RyR2 are expressed, whereas RyR3 is predominantly expressed in HCT116 colon cancer cells. RyR channel dysfunction or dysregulation has been implicated in many musculoskeletal disorders, and myocardial diseases associated with many mutations in RYR genes have been reported (Bellinger et al., 2009). RyR channels are tightly regulated by binding of tetrameric FK binding proteins 12.0 to the partially opened tetrameric receptor complex (Ahern et al., 1994). In the striated muscle cells, RyR channels are tightly regulated by binding to FKBP proteins in a stoichiometric ratio. The complex is destabilized by FKBP dissociation, implicating $Ca^{2+}$ mishandling, which is associated with cardiac and skeletal myopathies (Bellinger et al., 2008; Chelu et al., 2004).

Protein kinase A (PKA)-mediated phosphorylation of channel proteins reduces the affinity of the tetrameric complex for binding to FKBP tetramers thus causing a dysregulated or "leaky" channel (Ahern et al., 1994; Dirksen and Avila, 2002; Ivarsson et al., 2019; Marx et al., 2000). Our results show that the steady-state levels of both FKBP 12.0 proteins are markedly reduced (Figure S5) in cells with mitochondrial dysfunction. Based on this, we propose that a combination of increased RyR channel proteins and reduction of regulatory FKBP subunits results in the assembly of leaky channels, which result in increased $[Ca^{2+}]_c$. The possible involvement of RyR $Ca^{2+}$ channel function was further tested in two ways: first, RyR channel mRNA KD in mtDNA-depleted cells aborted the expression of MtRS markers including *Cn*, *IGF1R,* and *cathepsin L*. Furthermore, *RyR* mRNA KD also reduced the invasive potential of mtDNA-depleted C2C12 cells as tested by wound healing assay (Figure S4). In the second approach, the use of ryanodine, a specific antagonist of the RyR channel, essentially abrogated the increase in $[Ca^{2+}]_c$ (data not shown), activation of Cn, and the invasive property of mtDNA-depleted C2C12 cells. We, therefore, provide direct and rigorous proof for the involvement of activated RyR $Ca^{2+}$ channels in inducing MtRS.

Results presented here also show that mitochondrial $Ca^{2+}$ clearance is severely curtailed in cells with mitochondrial dysfunction (mtDNA depletion or CcO subunit KD). It is noteworthy that dysfunctional mitochondria also showed lower levels of mitochondrial uniporter protein MCU, although other members of uniporter complex such as MICU1 and EMRE are affected in a variable, cell-specific manner. In this regard, cells with mitochondrial defect show impaired uniporter complex and altered $Ca^{2+}$ clearance as shown by Mootha's group by shRNA-mediated KD of *MCU1* uniporter protein (Bick et al., 2012; Kamer and Mootha, 2015). Taken together, the results of this study provide mechanistic details of MtRS with respect to altered $Ca^{2+}$ release from ER and altered $Ca^{2+}$ clearance from mitochondria as the basis of Cn activation at the point of initiation of MtRS.

## Limitations of the Study

Although we present evidence for the upregulation of MtRS marker genes in both MCU1-depleted and MCU1-deleted mtDNA-depleted cells, a more comprehensive proteomic analysis and gene expression analyses would have been more informative. We plan to carry out these analyses in our future experiments. The FKBP binding to tetrameric RyR channel protein can be affected either by reduced steady-state levels of FKBP proteins or PKA-mediated phosphorylation of RyR channel proteins. Based on lower steady-state levels of FKBP, we suggested the former possibility. However, we cannot exclude the possibility of RyR subunit phosphorylation, which may also be the reason for the reduced affinity for the FKBP12, and this needs to be investigated. The $Ca^{2+}$ leak or mishandling due to dysregulation of RyR channels has been well documented in cardiac and skeletal myopathies, as discussed earlier in the article. In this respect, it would be interesting to study the possible activation of MtRS and its role in these muscle disease models.

## Resource Availability

### Lead Contact

Further information and requests for resources and reagents should be directed to and will be fulfilled by the Lead Contact, Narayan Avadhani (narayan@vet.upenn.edu).

### Materials Availability

All unique/stable reagents generated in this study are available from the Lead Contact with a completed Materials Transfer Agreement.

*Date and Code Availability*

No custom code, software, or algorithm was used in this research.

## METHODS

All methods can be found in the accompanying Transparent Methods supplemental file.

## SUPPLEMENTAL INFORMATION

Supplemental Information can be found online at https://doi.org/10.1016/j.isci.2020.101370.

## AUTHOR CONTRIBUTIONS

N.G.A., G.H., and G.C. conceptualized the project and obtained research support; A.R.C., S.S., and G.C. carried out the experiments; A.R.C. and S.S. analyzed the data; N.G.A., S.S., and A.R.C. wrote the paper; N.G.A., A.R.C., G.H., and G.C. edited the manuscript.

## DECLARATION OF INTERESTS

The authors declare no competing interests.

## REFERENCES

Ahern, G.P., Junankar, P.R., and Dulhunty, A.F. (1994). Single channel activity of the ryanodine receptor calcium release channel is modulated by FK-506. FEBS Lett. *352*, 369–374.

Amuthan, G., Biswas, G., Ananadatheerthavarada, H.K., Vijayasarathy, C., Shephard, H.M., and Avadhani, N.G. (2002). Mitochondrial stress-induced calcium signaling, phenotypic changes and invasive behavior in human lung carcinoma A549 cells. Oncogene *21*, 7839–7849.

Amuthan, G., Biswas, G., Zhang, S.Y., Klein-Szanto, A., Vijayasarathy, C., and Avadhani, N.G. (2001). Mitochondria-to-nucleus stress signaling induces phenotypic changes, tumor progression and cell invasion. EMBO J. *20*, 1910–1920.

Arnould, T., Vankoningsloo, S., Renard, P., Houbion, A., Ninane, N., Demazy, C., Remacle, J., and Raes, M. (2002). CREB activation induced by mitochondrial dysfunction is a new signaling pathway that impairs cell proliferation. EMBO J. *21*, 53–63.

Bagur, R., and Hajnoczky, G. (2017). Intracellular Ca(2+) sensing: its role in calcium homeostasis and signaling. Mol. Cell *66*, 780–788.

Baughman, J.M., Perocchi, F., Girgis, H.S., Plovanich, M., Belcher-Timme, C.A., Sancak, Y., Bao, X.R., Strittmatter, L., Goldberger, O., Bogorad, R.L., et al. (2011). Integrative genomics identifies MCU as an essential component of the mitochondrial calcium uniporter. Nature *476*, 341–345.

Bellinger, A.M., Mongillo, M., and Marks, A.R. (2008). Stressed out: the skeletal muscle ryanodine receptor as a target of stress. J. Clin. Invest. *118*, 445–453.

Bellinger, A.M., Reiken, S., Carlson, C., Mongillo, M., Liu, X., Rothman, L., Matecki, S., Lacampagne, A., and Marks, A.R. (2009). Hypernitrosylated ryanodine receptor calcium release channels are leaky in dystrophic muscle. Nat. Med. *15*, 325–330.

Bick, A.G., Calvo, S.E., and Mootha, V.K. (2012). Evolutionary diversity of the mitochondrial calcium uniporter. Science *336*, 886.

Biswas, G., Adebanjo, O.A., Freedman, B.D., Anandatheerthavarada, H.K., Vijayasarathy, C., Zaidi, M., Kotlikoff, M., and Avadhani, N.G. (1999). Retrograde Ca2+ signaling in C2C12 skeletal myocytes in response to mitochondrial genetic and metabolic stress: a novel mode of inter-organelle crosstalk. EMBO J. *18*, 522–533.

Biswas, G., Anandatheerthavarada, H.K., and Avadhani, N.G. (2005a). Mechanism of mitochondrial stress-induced resistance to apoptosis in mitochondrial DNA-depleted C2C12 myocytes. Cell Death Differ. *12*, 266–278.

Biswas, G., Guha, M., and Avadhani, N.G. (2005b). Mitochondria-to-nucleus stress signaling in mammalian cells: nature of nuclear gene targets, transcription regulation, and induced resistance to apoptosis. Gene *354*, 132–139.

Biswas, G., Srinivasan, S., Anandatheerthavarada, H.K., and Avadhani, N.G. (2008a). Dioxin-mediated tumor progression through activation of mitochondria-to-nucleus stress signaling. Proc. Natl. Acad. Sci. U S A *105*, 186–191.

Biswas, G., Tang, W., Sondheimer, N., Guha, M., Bansal, S., and Avadhani, N.G. (2008b). A distinctive physiological role for IkappaBbeta in the propagation of mitochondrial respiratory stress signaling. J. Biol. Chem. *283*, 12586–12594.

Brillantes, A.B., Ondrias, K., Scott, A., Kobrinsky, E., Ondriasova, E., Moschella, M.C., Jayaraman, T., Landers, M., Ehrlich, B.E., and Marks, A.R. (1994). Stabilization of calcium release channel (ryanodine receptor) function by FK506-binding protein. Cell *77*, 513–523.

Butow, R.A., and Avadhani, N.G. (2004). Mitochondrial signaling: the retrograde response. Mol. Cell *14*, 1–15.

Carden, T., Singh, B., Mooga, V., Bajpai, P., and Singh, K.K. (2017). Epigenetic modification of miR-663 controls mitochondria-to-nucleus retrograde signaling and tumor progression. J. Biol. Chem. *292*, 20694–20706.

Cardenas, C., Miller, R.A., Smith, I., Bui, T., Molgo, J., Muller, M., Vais, H., Cheung, K.H., Yang, J., Parker, I., et al. (2010). Essential regulation of cell

bioenergetics by constitutive InsP3 receptor Ca2+ transfer to mitochondria. Cell *142*, 270–283.

Chelu, M.G., Danila, C.I., Gilman, C.P., and Hamilton, S.L. (2004). Regulation of ryanodine receptors by FK506 binding proteins. Trends Cardiovasc. Med. *14*, 227–234.

Chowdhury, A.R., Long, A., Fuchs, S.Y., Rustgi, A., and Avadhani, N.G. (2017). Mitochondrial stress-induced p53 attenuates HIF-1alpha activity by physical association and enhanced ubiquitination. Oncogene *36*, 397–409.

Clapham, D.E. (2007). Calcium signaling. Cell *131*, 1047–1058.

Demaurex, N., and Nunes, P. (2016). The role of STIM and ORAI proteins in phagocytic immune cells. Am. J. Physiol. Cell Physiol. *310*, C496–C508.

Desideri, E., Vegliante, R., and Ciriolo, M.R. (2015). Mitochondrial dysfunctions in cancer: genetic defects and oncogenic signaling impinging on TCA cycle activity. Cancer Lett. *356*, 217–223.

Dirksen, R.T., and Avila, G. (2002). Altered ryanodine receptor function in central core disease: leaky or uncoupled Ca(2+) release channels? Trends Cardiovasc. Med. *12*, 189–197.

Duchen, M.R. (1999). Contributions of mitochondria to animal physiology: from homeostatic sensor to calcium signalling and cell death. J. Physiol. *516* (Pt 1), 1–17.

Fang, H., Shen, L., Chen, T., He, J., Ding, Z., Wei, J., Qu, J., Chen, G., Lu, J., and Bai, Y. (2010). Cancer type-specific modulation of mitochondrial haplogroups in breast, colorectal and thyroid cancer. BMC Cancer *10*, 421.

Franzini-Armstrong, C. (2007). ER-mitochondria communication. How privileged? Physiol. (Bethesda) *22*, 261–268.

Friedman, J.R., and Nunnari, J. (2014). Mitochondrial form and function. Nature *505*, 335–343.

Friis, R.M., Glaves, J.P., Huan, T., Li, L., Sykes, B.D., and Schultz, M.C. (2014). Rewiring AMPK and mitochondrial retrograde signaling for metabolic control of aging and histone acetylation in respiratory-defective cells. Cell Rep. *7*, 565–574.

Giorgi, C., De Stefani, D., Bononi, A., Rizzuto, R., and Pinton, P. (2009). Structural and functional link between the mitochondrial network and the endoplasmic reticulum. Int. J. Biochem. Cell Biol. *41*, 1817–1827.

Goffart, S., and Wiesner, R.J. (2003). Regulation and co-ordination of nuclear gene expression during mitochondrial biogenesis. Exp. Physiol. *88*, 33–40.

Green, D.R., and Wang, R. (2010). Calcium and energy: making the cake and eating it too? Cell *142*, 200–202.

Guha, M., and Avadhani, N.G. (2013). Mitochondrial retrograde signaling at the crossroads of tumor bioenergetics, genetics and epigenetics. Mitochondrion *13*, 577–591.

Guha, M., Pan, H., Fang, J.K., and Avadhani, N.G. (2009). Heterogeneous nuclear ribonucleoprotein A2 is a common transcriptional coactivator in the nuclear transcription response to mitochondrial respiratory stress. Mol. Biol. Cell *20*, 4107–4119.

Guha, M., Srinivasan, S., Biswas, G., and Avadhani, N.G. (2007). Activation of a novel calcineurin-mediated insulin-like growth factor-1 receptor pathway, altered metabolism, and tumor cell invasion in cells subjected to mitochondrial respiratory stress. J. Biol. Chem. *282*, 14536–14546.

Guha, M., Srinivasan, S., Johnson, F.B., Ruthel, G., Guja, K., Garcia-Diaz, M., Kaufman, B.A., Glineburg, M.R., Fang, J., Nakagawa, H., et al. (2018). hnRNPA2 mediated acetylation reduces telomere length in response to mitochondrial dysfunction. PLoS One *13*, e0206897.

He, Y., Wu, J., Dressman, D.C., Iacobuzio-Donahue, C., Markowitz, S.D., Velculescu, V.E., Diaz, L.A., Jr., Kinzler, K.W., Vogelstein, B., and Papadopoulos, N. (2010). Heteroplasmic mitochondrial DNA mutations in normal and tumour cells. Nature *464*, 610–614.

Ishikawa, K., Takenaga, K., Akimoto, M., Koshikawa, N., Yamaguchi, A., Imanishi, H., Nakada, K., Honma, Y., and Hayashi, J. (2008). ROS-generating mitochondrial DNA mutations can regulate tumor cell metastasis. Science *320*, 661–664.

Ivarsson, N., Mattsson, C.M., Cheng, A.J., Bruton, J.D., Ekblom, B., Lanner, J.T., and Westerblad, H. (2019). SR Ca(2+) leak in skeletal muscle fibers acts as an intracellular signal to increase fatigue resistance. J. Gen. Physiol. *151*, 567–577.

Kamer, K.J., and Mootha, V.K. (2015). The molecular era of the mitochondrial calcium uniporter. Nat. Rev. Mol. Cell Biol. *16*, 545–553.

Klee, C.B., Crouch, T.H., and Krinks, M.H. (1979). Calcineurin: a calcium- and calmodulin-binding protein of the nervous system. Proc. Natl. Acad. Sci. U S A *76*, 6270–6273.

Mammucari, C., Gherardi, G., and Rizzuto, R. (2017). Structure, activity regulation, and role of the mitochondrial calcium uniporter in health and disease. Front. Oncol. *7*, 139.

Marx, S.O., Reiken, S., Hisamatsu, Y., Jayaraman, T., Burkhoff, D., Rosemblit, N., and Marks, A.R. (2000). PKA phosphorylation dissociates FKBP12.6 from the calcium release channel (ryanodine receptor): defective regulation in failing hearts. Cell *101*, 365–376.

Meissner, G. (2010). Regulation of ryanodine receptor ion channels through posttranslational modifications. Curr. Top. Membr. *66*, 91–113.

Mishra, J., Jhun, B.S., Hurst, S., J, O.U., Csordas, G., and Sheu, S.S. (2017). The mitochondrial Ca(2+) uniporter: structure, function, and pharmacology. Handb Exp. Pharmacol. *240*, 129–156.

Pessah, I.N., Stambuk, R.A., and Casida, J.E. (1987). Ca2+-activated ryanodine binding: mechanisms of sensitivity and intensity modulation by Mg2+, caffeine, and adenine nucleotides. Mol. Pharmacol. *31*, 232–238.

Rizzuto, R., De Stefani, D., Raffaello, A., and Mammucari, C. (2012). Mitochondria as sensors and regulators of calcium signalling. Nat. Rev. Mol. Cell Biol. *13*, 566–578.

Srinivasan, S., and Avadhani, N.G. (2007). Hypoxia-mediated mitochondrial stress in RAW264.7 cells induces osteoclast-like TRAP-positive cells. Ann. N. Y Acad. Sci. *1117*, 51–61.

Srinivasan, S., Guha, M., Dong, D.W., Whelan, K.A., Ruthel, G., Uchikado, Y., Natsugoe, S., Nakagawa, H., and Avadhani, N.G. (2016). Disruption of cytochrome c oxidase function induces the Warburg effect and metabolic reprogramming. Oncogene *35*, 1585–1595.

Tait, S.W., and Green, D.R. (2012). Mitochondria and cell signalling. J. Cell Sci *125*, 807–815.

Taylor, C.W., and Tovey, S.C. (2010). IP(3) receptors: toward understanding their activation. Cold Spring Harb Perspect. Biol. *2*, a004010.

Visch, H.J., Koopman, W.J., Zeegers, D., van Emst-de Vries, S.E., van Kuppeveld, F.J., van den Heuvel, L.W., Smeitink, J.A., and Willems, P.H. (2006). Ca2+-mobilizing agonists increase mitochondrial ATP production to accelerate cytosolic Ca2+ removal: aberrations in human complex I deficiency. Am. J. Physiol. Cell Physiol *291*, C308–C316.

Yang, D., and Kim, J. (2019). Mitochondrial retrograde signalling and metabolic alterations in the tumour microenvironment. Cells *8*, 275.

Yong, C.Q.Y., and Tang, B.L. (2018). A mitochondrial encoded messenger at the nucleus. Cells *7*, 105.

**Supplemental Information**

# Dysregulation of RyR Calcium Channel Causes

# the Onset of Mitochondrial Retrograde Signaling

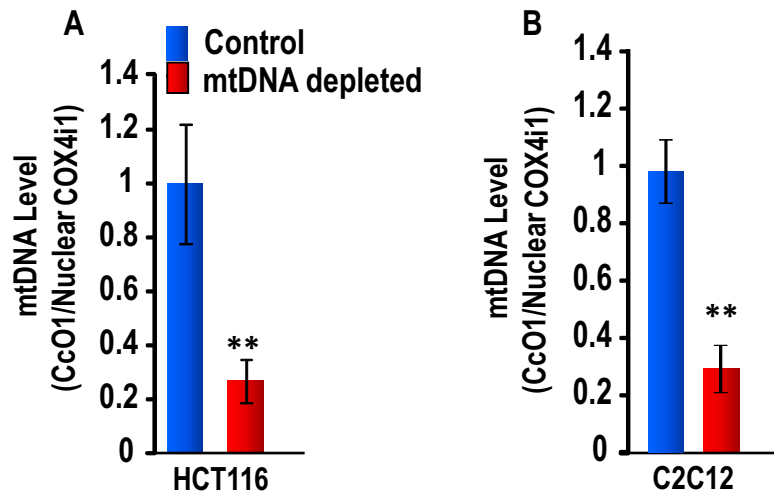Anindya Roy Chowdhury, Satish Srinivasan, György Csordás, György Hajnóczky, and Narayan G. Avadhani

**Figure S1**: **mtDNA content in Depleted HCT116 and C2C12 Cells**. Related to Figure 1 and 2
mtDNA depletion in HCT116 carcinoma cells (A) and C2C12 (B) cells were carried out by treating with 2′,3′-Dideoxycytidine (ddC) and ethidium bromide (EtBr) as described in the Methods section. mtDNA contents were measured using qRT-PCR as described before (see Transparent Methods section). Statistical comparisons were performed by one-way ANOVA with Tukey's multiple-comparison test, and data are presented as the treatment group versus no-treatment control. In all experiments, error bars represent as mean ±S.D. (**p < 0.01). Each assay was done in triplicate.
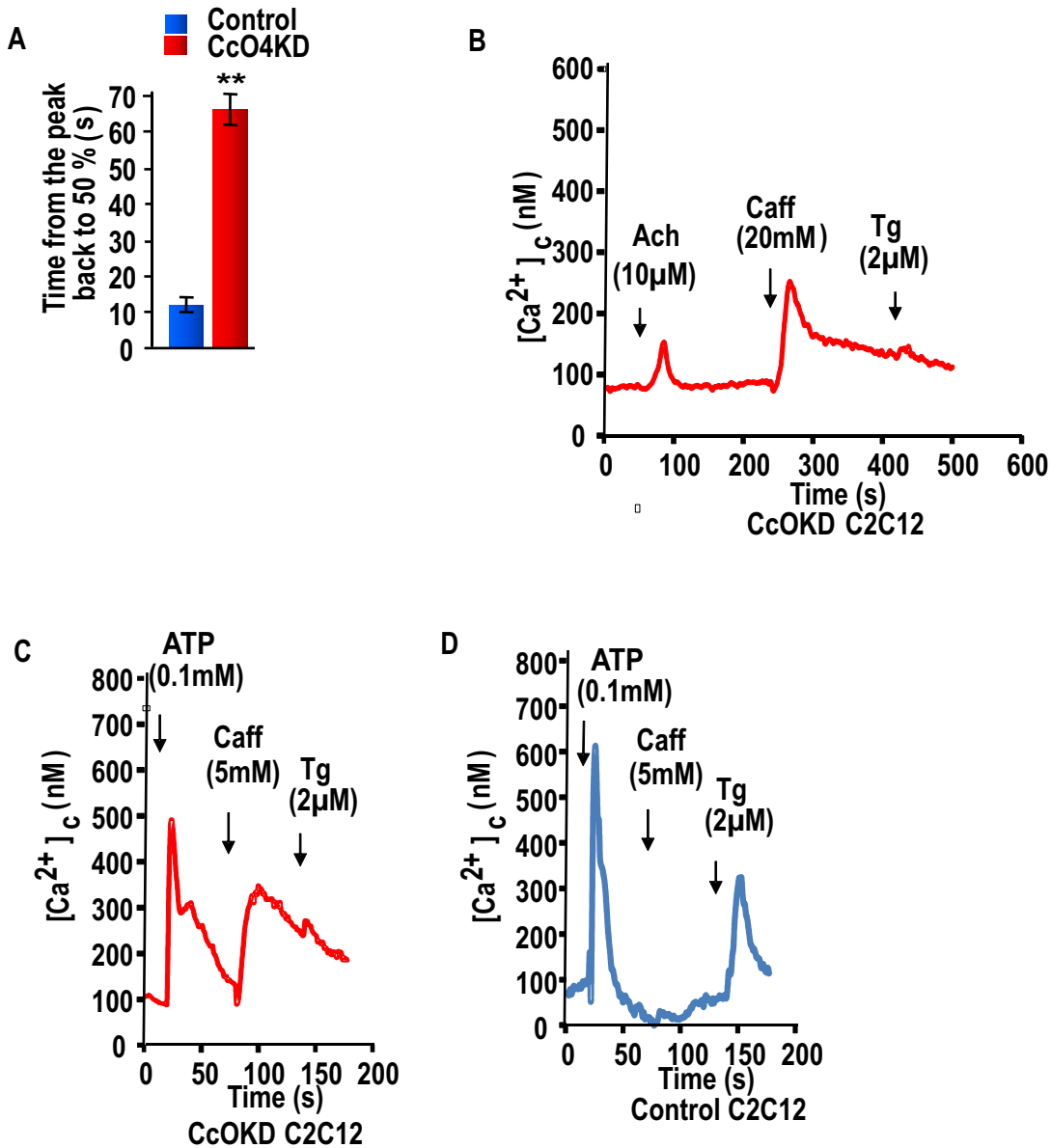
**Figure S2: Activation of RyR, but not IP3 channels in CcO KD C2C12 cells.** Related to Figure 1

Details of Ca2+ clearance, as described in Figs 1 and 2. A bar diagram of [Ca2+]c clearance from a peak to 50 % was measured after acetylcholine (Ach) addition (n = 30, p<0.001) (A). Statistical comparisons were performed by one-way ANOVA with Tukey's multiple-comparison test, and data are presented as the treatment group versus no-treatment control. In all experiments, error bars represent as mean ±S.D. (**p < 0.01). Each assay was done in triplicate. B, traces show the average response of 3 different runs (n=20 cells/run) following the addition of the different agonists in CcO4KD cells for a longer period. C and D show the Ca2+ release in CcO4KD and control C2C12 cells in response to ATP (0.1 mM) with the following addition of 5 mM caffeine (Caff). Recorded data were further analyzed by Spectralyzer LSMDeluxe version 2009092525 software to subtract the background fluorescence before calculating the F380/340 ratio and finally represented as nM. Fig. B and C show that caffeine evokes Ca2+ release even after acetylcholine treatment or treatment with ATP in CcO4KD cells. However, in control cells, caffeine is unable to induce the release of Ca2+ following ATP treatment (Fig. D).
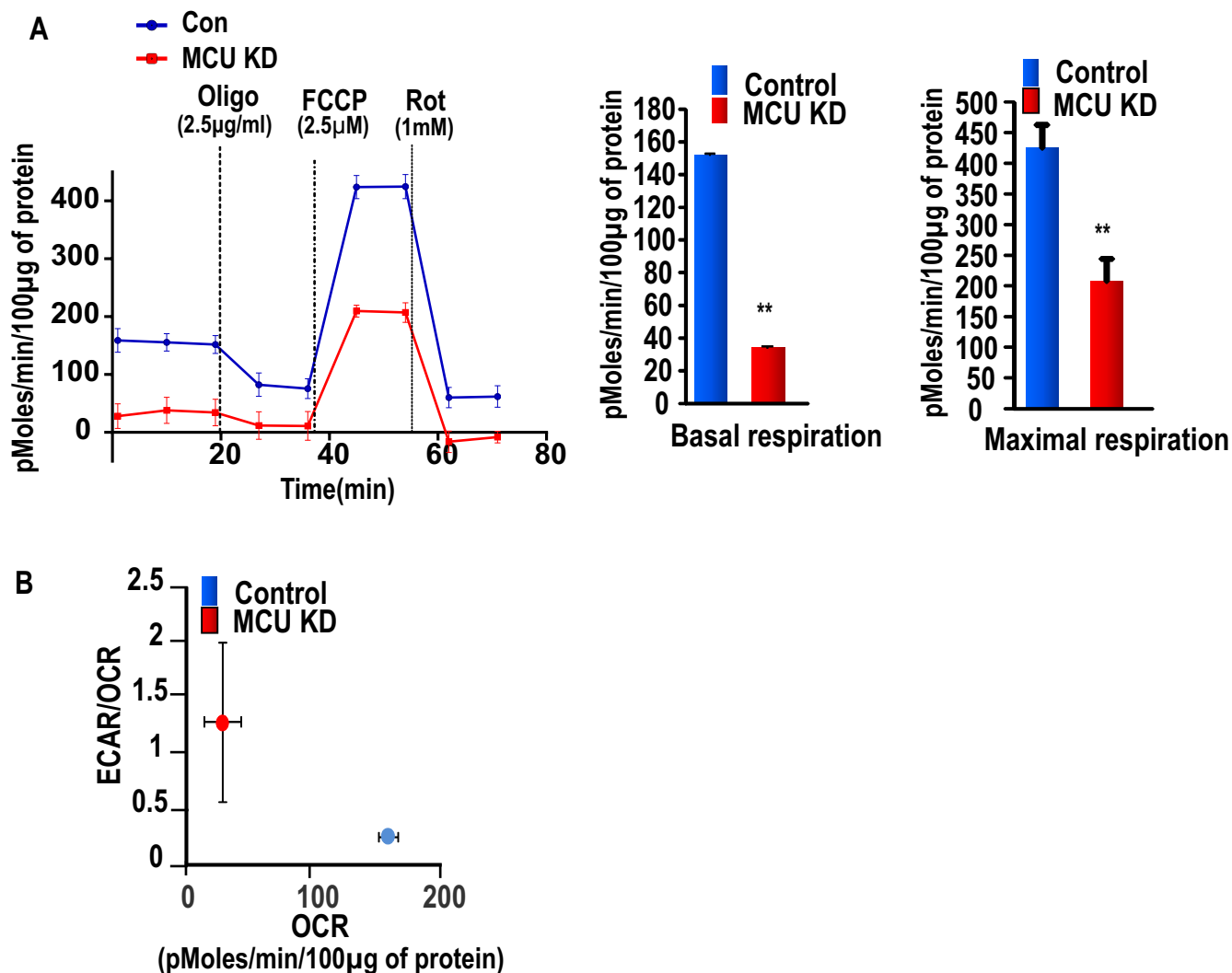
**Figure S3: Metabolic patterns of MCU KD C2C12 cells.** Related to Figure 5

Respiratory controls were measured using a Seahorse FX-24 analyzer. A. shows the respiratory profiles of control and MCU KD HCT116 cells and shows reduced basal and maximal respiration in MCU KD cells. B. shows the ECAR:OCR ratio in control and MCU KD cells. Results show a preference for glycolysis over oxidative phosphorylation. Statistical comparisons are performed by one-way ANOVA with Tukey's multiple-comparison test, and data are presented as the treatment group versus no-treatment control. In all experiments error bars represent as ±SEM ($**p < 0.01$). Each assay was done in triplicate.
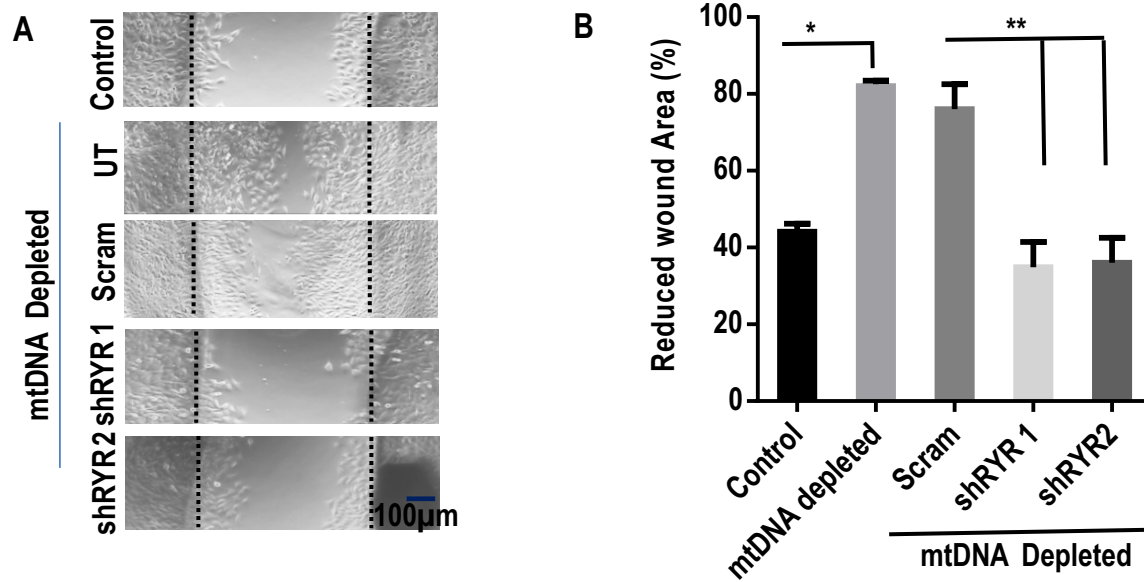
**Figure S4: Wound healing assay in mtDNA depleted and RYR mRNA silenced C2C12 Cells.**
Related to Figure 7
A. Representative images of scratch wound healing assay of control C2C12 cells, mtDNA depleted cells, and mtDNA depleted/RyR silenced cells. shRNAs targeting all three RyR genes were used. B. quantitation of scratched areas covered by cells reflecting proliferation. In all experiments error bars represent ±S.D. (n=3, *p < 0.05, **p < 0.01).
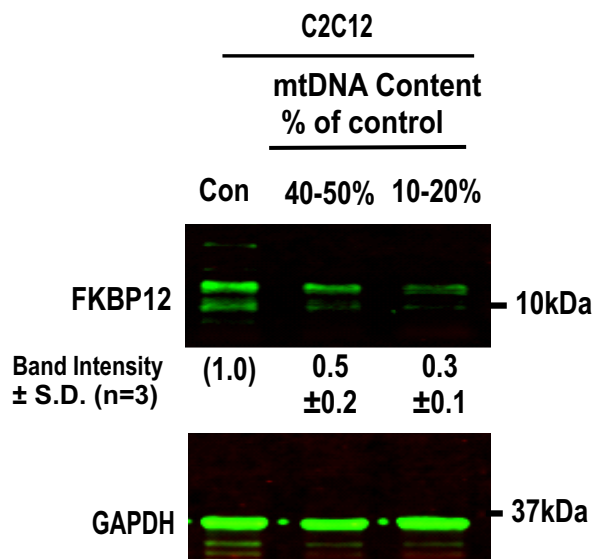
**Figure S5: Analysis of FKBP protein in mtDNA depleted C2C12 cells.** Related to Figure 7
Immunoblot analysis of FKBP protein from control and mtDNA depleted C2C12 cells. Total cell extracts of two different mtDNA depleted C2C12 clones showing 40-50% and 10-20% mtDNA contents were analyzed by Western blot analysis using the FKBP12 antibody. 30 µg proteins from whole cell extracts were used in each case. Immunoblots (n=3) were developed using respective primary (1:1000 dilution) and 1:10000 dilutions of secondary antibodies. The blots were imaged as described in the Transparent Methods. GAPDH was used as a loading control.

**Supplemental Table S1**

**List of qRT-PCR Primers** Related to Figure 1, 2,5 and 6

| | |
|---|---|
| huMCU | F= GGGTGGCCTTGCCTACATG<br>R= GGTAAGCCGGGCCAAAA |
| huMICU1 | F= ACTGGCTGTGGGTTCTCGAT<br>R= GTCTTCGCCGGATCTGGAT |
| huEMRE | F= CAGCGGCGCCATTTTG<br>R= CGGAGAAGGCCGAAGGA |
| huRyR1 | F= CTTCTCTAATCCGTGGCAATCG<br>R= ACCAGCCAGTCCAAGTTTGTG |
| huCcOI | F= CCCCGCATAAACAACATAAGC<br>R= CAGATGCGAGCAGGAGTAGGA |
| huCOX4i1 | F= GGGCGGTGCCATGTTCT<br>R= CATAGTGCTTCTGCCACATGA |
| hubeta- Actin | F= CACCATTGGCAATGAGCGGTTC<br>R= AGGTCTTTGCGGATGTCCACGT |
| muMCU | F= AAAGGAGCCAAAAAGTCACG<br>R= AACGGCGTGAGTTACAAACA |
| muMICU1 | F= GTCGAACTCTCGGACCATGT<br>R= CAAAGTCCCAGGCAGTTTCT |
| muEMRE | F= CGGGACACTCATCAGCAAGA<br>R= CCTCTGGGACAAAAATGTCATG |
| muCcOI | F= TGCTAGCCGCAGGCATTACT<br>R= GCGGGATCAAAGAAAGTTGTG |
| muCOX4i1 | F= GCGCCATGTCTGTCTTTAATCTT<br>R= GCGGGCTTTATGCGTTTACA |
| muIGF1R | F= CAGATGGCTGGAGAGATTGCA<br>R= GTGGACGAACTTGTTGGCATT |
| muRYR1 | F= TCCCGATCCATGACTGACAA<br>R= CCCTGTTGCGTCTTCCTGTAA |
| muRYR2 | F= TGCCAAGCGCATCGAAA<br>R=TCCCCGCCCTCATTGAC |
| muRYR3 | F= CCGTCTTCGTAAACAGCGAAA<br>R= AGCAGTCCGTTGCCTCCTT |
| muIP3-1R | F= GCTTGCTGCTTTTTGATTTAGTGTAC<br>R= GACCGCTGTCAAGATGATGGA |
| muIP3-3R | F= CCTCCCCCAAGGCAAACT<br>R= GACCTAGCATCCTCTAAGGCACTAA |
| muGlut4 | F= CCCACAAGGCACCCTCAACTA<br>R= TCATGCCACCCACAGAGAAG |
| mubeta-Actin | F=  ATGGTGGGAATGGGTCAGAA<br>R= CCATGTCGTCCCAGTTGGTAA |

**Transparent Methods**

**Cell Lines and Culture Conditions Murine**

C2C12 skeletal myoblasts (ATCC CRL1772), human colon cancer HCT116 cells (ATCC CCL-247), and human embryonic kidney HEK293T cells (ATCC® ACS-4500™) were grown in Dulbecco's Modified Eagle's medium (GIBCO, Thermo Fisher Scientific, Waltham, MA) supplemented with 10% FBS and 0.1% Penicillin Streptomycin. Partial depletion of mtDNA was carried out either by ethidium bromide treatment (100 ng/ml, for five passages) or by treating with 10 μM ddC as described before (Chen and Cheng, 1989; Chowdhury et al., 2017). Selected clones with mtDNA contents reduced by 70-80% were grown in the presence of 1 mM sodium pyruvate and 50 μg/ml uridine. The mtDNA contents were measured by quantitative real time PCR from total genomic DNA (Chowdhury et al., 2017).

shRNA mediated depletion of *MCU* was carried out in C2C12 cells using lentiviral based shRNA constructs obtained from Santa Cruz (Santa Cruz Biotechnology Inc., Dallas, USA*).* Briefly, virus particles were collected after 48 to 72 h of transfection in 293T cells with the plasmid using FugeneHD (Promega Corporation, USA) as a transfection agent. C2C12 cells grown to 60% confluence were than infected with filtered virus containing medium in the presence of 8 μg/ml polybrene. One day after infection, cells were treated with 1.2 μg/ml Puromycin for the selection of stable clones.

**CcO subunits IVi1 and RYR Ca$^{2+}$ channel mRNA silencing in C2C12 cells**

Stable C2C12 cell lines expressing shRNA against subunit IVi1 were generated using the pSilencer 2.0 vector, as described before (Galati et al., 2009). In brief, an oligonucleotide specific for this sequence was synthesized and cloned into the pSilencer 2.0 vector according to the manufacturer's protocol (Ambion, Thermos Fisher Scientific, Waltham, MA).

The shRNA expression cassettes procured from OriGene Technologies (Rockville, MD) were used to silence the *RYR*1 gene (Catalogue # TL501959) in C2C12 cells. Stable cell lines expressing shRNA were generated by puromycin selection (1.2 μg/ml).

Simultaneously a scrambled sequence cassette was cloned in the same vector as a negative control.

**Mitochondrial Ca²⁺ clearance assay**

Mitochondrial calcium clearance was assayed in cells permeabilized with saponin using a method to prserve mitochondrial functional integrity (Csordas and Hajnoczky, 2003). In brief, cells were harvested by trypsin-EDTA and washed with Ca²⁺-free extracellular buffer (ECM: 120 mM NaCl, 20 mM Na-HEPES, 5 mM KCl, 1.0 mM KH₂PO₄, 0.1 mM EGTA/Tris and 20 mM HEPES-NaOH pH 7.4), and incubated at 37°C for 40-45 min to fully deplete intracellular Ca²⁺ stores. Aliquots of 6 x 10⁶ cells were kept in ice cold Ca²⁺ free ECM buffer on ice. Before permeabilization, cells were spun down at 100g for 5 min, and the supernatant was removed carefully. For cell permeabilization and fluorescence recordings a nominally calcium-free intracellular medium, ICM was used that was composed of 120 mM KCl, 10 mM NaCl, 1 mM KH₂PO₄, 5% Dextran, 20 mM HEPES–Tris pH 7.2 and it was passed through a Chelex column (Chelex 100 resins, BioRad). Cells were resuspended in the pre-warmed ICM supplemented with protease inhibitors (Leupeptin, Pepstatin, and Antipain 1 µg/ml each, from sigma), 2 mM Mg-ATP, 40 µg/ml saponin, EGTA/Tris 5 µM and incubated for 5 min at 37°C.  After permeabilization cells were again spun down and resuspended in fresh ICM supplemented with protease inhibitors, 2 mM Mg-ATP, and 2 mM succinate/Tris. The mitochondrial Ca²⁺ influx was measured in the presence of thapsigargin, a sarco/endoplasmic reticulum Ca²⁺-ATPase (SERCA) inhibitor. To measure both [Ca2+]c and mitochondrial membrane potential (ΔΨm), 1.5 µM TMRM and Fura2-FF/FA simultaneously were added to the assay buffer. Fluorescence measurements were carried out in a stirred thermostated cuvette at 35°C using a multi-wavelength excitation dual wavelength-emission fluorimeter (Delta RAM, PTI) using 340- and 380-nm excitation and 500-nm emission and 540-nm excitation and 580-nm emission for TMRE.  Calibration of the [Ca²⁺] was performed at the end of the measurements by sequential addition of 1mM CaCl₂ and 10mM EGTA/Tris (pH8.5).

**Live cell calcium recording**

For live cell imaging. the cells on a coverslip were pre-incubated with a serum-free extracellular buffer (SFB, 121 mM NaCl, 5 mM NaHCO$_3$, 10 mM Na-HEPES, 4.7 mM KCl, 1.2 mM KH$_2$PO$_4$, 1.2 mM MgSO$_4$, 2 mM CaCl$_2$, 10 mM glucose, pH7.4) containing 2% BSA at room temperature (Csordas and Hajnoczky, 2003). After 20 min, 0.003% pluronic acid F-127 and 5 µM Fura-2AM were added and further incubated for 5 min. SFB was then replaced with fresh 1 ml 2% BSA-SFB supplemented with 0.1 mM sulfinpyrazone. After 10 min incubation, 20nM TMRE was added and re-incubated for another 15 min. Subsequent to TMRE loading, coverslips were washed into 0.25% BSA-SFB running buffer (0.25% BSA-SFB + 0.1 mM sulfinpyrazone + 2 nM TMRE) in thermostated imaging chamber. Fluorescence imaging of [Ca$^{2+}$]$_c$ and $\Delta\Psi$m was carried out using a Leica inverted epifluorescence microscope. [Ca$^{2+}$]$_c$ with Fura2 was recorded with 340 nm and 380 nm excitation and 510-nm emission. Excitation 545nm and emission 580nm for TMRE were used. The Ca$^{2+}$-saturated and Ca$^{2+}$-free Fura2 fluorescences were assessed in vitro in ICM using the same microscope settings to convert the fluorescence ratio values to molar values of [Ca$^{2+}$].

**mRNA quantitation by real time PCR**

Total RNA was isolated using TRIzol reagent as per the vendor's protocol (Invitrogen). cDNA was generated from 1 µg of RNA using the cDNA Archive kit from Applied Biosystems (Thermo Fisher Scientific, Waltham, MA), and 25 ng of this cDNA was used as template per reaction. mRNA levels were quantified using SYBR Green (Applied Biosystems) in a Quant Studio 6 sequence detection system (Applied Biosystems). Data were normalized to β-actin as endogenous controls, and relative expression of target genes were expressed in $2^{-\Delta\Delta Ct}$ methods, and used primers are listed in Supplemental Table 1.

**Calcineurin assay**

Cn activity was measured using the Cn cellular activity assay kit (Enzo Life sciences, Farmingdale, NY, USA) according to the manufacturer's suggested protocol. The kit measures free phosphate released from the Cn specific RII phosphopeptide. Free

phosphate released was measured using malachite green at 620 nm. Cn specific phosphatase activity was calculated by subtracting activity in the presence of EGTA from total phosphatase activity.

**Measurement of Respiration rates**

Mitochondrial respiration was measured using an XF24 extracellular flux analyzer (Seahorse Biosciences, North Billerica, MA) which detects rapid, real time changes in cellular respiration and glycolysis rates (Wu et al., 2007). Analysis of extracellular acidification rate (ECAR) reflects lactate excretion and serves as an indirect measure of glycolysis rate, while oxygen consumption rate (OCR) reflects cellular respiration. The Seahorse XF24 Extracellular Flux Analyzer continuously measures oxygen concentration and proton flux ($H^+$) in the cell supernatant over time. These measurements are converted in OCR and ECAR values, which enable direct quantification of mitochondrial oxidative respiration and glycolysis. For measuring respiratory rates, cells were seeded in XF24 microplates (25,000 cells/well) the day before the measurements in the XF24 medium. All analyses were performed following the manufacturer-suggested protocol, and the observed rates are reported in pMoles/min/100µg of protein for OCR and mpH/min/100µg of protein for ECAR. The experiment was repeated three times.

**Immunoblot and Immunoprecipitation analysis**

All immunoblots were repeated three times. Whole-cell lysates were prepared by washing the cells with ice-cold PBS and lysing with lysis buffer (60 mM Tris-HCl pH 7.5, 150 mM NaCl, 10 mM $MgCl_2$, 2 mM EDTA, 10% glycerol, 1% Triton X-100, 10 mM NaF, 2 mM PMSF, and protease inhibitors,1 µg/ml each aprotinin, antipain, pepstatin, leupeptin, 1 mM sodium orthovanadate and 0.1 mM molybdic acid)**.** Proteins were resolved by 4 to 12.5% gradient SDS-PAGE, transferred on to a nitrocellulose membrane (BioRad), and developed with appropriate primary antibodies. For immunoprecipitation assay cells suspended in RIPA assay buffer (10 mm Tris, 100 mm NaCl, 1 mm EDTA, 1 mm EGTA, 20 mm$Na_4P_2O_7$, 0.1mM sodium molybdate, 1% Triton X-100, 0.5% sodium deoxycholate, 0.1% SDS, 10% glycerol, 2mM PMSF, 50mM NaF, pH 7.5) and Protease & Phosphatase Inhibitor cocktail (1µg/ml concentration of aprotinin, antipain, leupeptin and pepstatin;

Sigma Aldrich). Protein lysates (500 µg) were incubated with protein A/G agarose (Santa Cruz Biotechnology, Inc.) in 500 µl of RIPA buffer at 4 °C for 1 h, to minimize nonspecific binding. The lysate was cleared at 20,000 rpm for 5min, and the supernatant fractions were incubated with RyR (Novus Biologicals, LLC; Cat# NB300-543) specific antibodies for overnight at 4 °C. Subsequently, protein G Sepharose was added to each sample and incubated at 4 °C for 1 h. Mouse IgG was used as a negative control. The immune complex was collected, washed with RIPA buffer, and subjected to SDS-PAGE (4% to 20% gradient gel) followed by transfer to nitrocellulose membrane. The antibody-reactive protein bands were detected by an Odyssey (LI-COR, Lincoln, NE, USA) infrared scanning system. The primary antibodies used in immunoblot experiments are: MICU1 (Cat# MBS9400198) procured from MyBiosource, San Diego, CA; MCU (Cat# HPA016480) from Sigma-Aldrich, St. Louis, MO; both C22orf32/EMRE (Cat# NBP1-84289) and RyR (Cat# NB300-543) procured from Novus Biologicals, LLC (Centennial, CO) which cross reacts with all three forms of RYR Channels (Airey et al., 1993), Littleton, CO; Cn (Cat# 07-068) EMD Millipore, Burlington, MA; GAPDH (Cat# 60004-1) from Proteintech (North America, Rosemont, IL), and FKBP12 (Cat# SC-6174) from Santa Cruz Biotechnology, Inc.

**Matrigel Invasion Assay**

Cell migration assay was performed in triplicates for each group using 24 well plate transwell chambers (8 µm pore, Corning, NY). Initially, 100 µl (200 µg/ml) corning matrigel matrix was used to coat the top part of the membrane. $2.5 \times 10^4$ cells / well were seeded for each group with required treatments, as mentioned in figures. 700 µl DMEM containing 20% FBS was kept in basolateral chambers and incubated for 14-16 h at 37 °C with 5% $CO_2$ incubator. Cells were then fixed with chilled methanol and incubated for 6 min in hematoxylin solution Gill 3 (Sigma-Aldrich, St. Louis, MO) for staining the cells. Non-invading cells were removed from the top of the Matrigel layer by a wet cotton swab. Images were captured by Olympus BX-61 upright microscope (Olympus) with a 10X objective lens. Five random visual fields were selected to count the cells and represented as the number of invading cells per field.

**Wound Healing Assay:**

The Control and RyR knocked down C2C12 cells, and also those transduced with a respective scrambled vector expressing cells were grown in confluent monolayer and to mimic a wound, a thin wound created by scratching with a P200 pipette tip. Images were collected at 0 h and 24 h under an inverted light microscope (Nikon, Japan). Cell migration was analyzed using NIH ImageJ software, and the area between the two boundaries of the scratch was calculated after 24 h growth.

**Statistical analysis**

Statistical analyses were carried out using Microsoft Excel or Graphpad prism Software. Statistical significance was determined by an unpaired two-tailed Student's $t$-test and paired when needed, and equality of variance was checked using a one-way ANOVA test. All the data for the *in vitro* experiments have been presented as means ± S.D. of at least three data points from three different experiments. *$p$-values ≤ 0.05 were considered statistically significant, and **$p$-values ≤ 0.01 were considered highly significant.

**Supplemental References:**

Chen, C.H., and Cheng, Y.C. (1989). Delayed cytotoxicity and selective loss of mitochondrial DNA in cells treated with the anti-human immunodeficiency virus compound 2',3'-dideoxycytidine. J Biol Chem *264*, 11934-11937.

Galati, D., Srinivasan, S., Raza, H., Prabu, S.K., Hardy, M., Chandran, K., Lopez, M., Kalyanaraman, B., and Avadhani, N.G. (2009). Role of nuclear-encoded subunit Vb in the assembly and stability of cytochrome c oxidase complex: implications in mitochondrial dysfunction and ROS production. Biochem J *420*, 439-449.

Csordas, G., and Hajnoczky, G. (2003). Plasticity of mitochondrial calcium signaling. J Biol Chem *278*, 42273-42282.

Wu, M., Neilson, A., Swift, A.L., Moran, R., Tamagnine, J., Parslow, D., Armistead, S., Lemire, K., Orrell, J., Teich, J*., et al.* (2007). Multiparameter metabolic analysis reveals a close link between attenuated mitochondrial bioenergetic function and enhanced glycolysis dependency in human tumor cells. Am J Physiol Cell Physiol *292*, C125-136.